



Assessing the climate change impact on the North African offshore surface wind and coastal low-level jet using coupled and uncoupled regional climate simulations

Pedro M. M. Soares¹ · Daniela C. A. Lima¹ · Alvaro Semedo² · Rita M. Cardoso¹ · William Cabos³ · Dmitry V. Sein^{4,5}

Received: 23 February 2018 / Accepted: 3 December 2018
© The Author(s) 2018

Abstract

The North African Coastal Low-Level Jet (NACLLJ) is a semi-permanent feature offshore the north western African coast, linked to the cold nearshore upwelling of the Canary Eastern Boundary Current system. Its main synoptic drivers are the Azores Anticyclone over the ocean and the inland Sahara thermal low. The coastal jet events occur in one of the world's most productive fisheries region, thus the evaluation of the effects of global warming in its properties is imperative. This study proposes an analysis of the annual and intra-annual attributes of the NACLLJ for two time periods 1976–2005 (historical) and 2070–2199 (future), resorting to coupled and uncoupled atmosphere–ocean simulations with the ROM model, as well as near surface offshore wind speed from the CORDEX–Africa ensemble. The future simulations follow the RCP8.5 greenhouse gas emissions scenario. Overall, the ROM coupled simulation presents the best performance in reproducing the present-climate near surface wind speed, offshore northwest Africa, compared to the remaining RCM simulations. The higher SST resolution in the coupled simulations favours much localised colder upwelling strips near the coast and consequently stronger jets. In future climate, a small increase in the surface wind speed is projected, mainly linked to the regions of coastal jet presence. The NACLLJ is projected to be more frequent and intense, encompassing larger areas. An increase of the jet seasonal frequencies of occurrence is projected for all seasons, which is larger from spring to autumn (up to 15, 16 and 22% more frequent, respectively). However, in some offshore areas the winter NACLLJ persistency is likely to double, relatively to present-climate. Higher inter-annual variability is also projected for the future NACLLJ seasonal frequencies. The strengthening of the coastal jet speeds is also significant, between 5 and 12% in all seasons. Additionally, the jet's diurnal cycle shows an increase in jet occurrence across the day, particularly in the mid and late afternoon.

Keywords Regional climate modelling · Coastal low-level wind jet · Africa · CORDEX · REMO–OASIS–MPIOM · Global warming

Electronic supplementary material The online version of this article (<https://doi.org/10.1007/s00382-018-4565-9>) contains supplementary material, which is available to authorized users.

✉ Pedro M. M. Soares
pmsoares@fc.ul.pt

¹ Instituto Dom Luiz (IDL), Faculdade de Ciências da Universidade de Lisboa, Campo Grande, Ed. C8 (3.26), 1749-016 Lisbon, Portugal

² Department of Water Science and Engineering, IHE-Delft, P.O. Box 3015, 2601 DA Delft, The Netherlands

1 Introduction

Regional and local climates along Eastern Boundary Current System (EBCS) regions are highly influenced by coastal atmosphere–land–ocean interaction processes, namely by the land–ocean temperature contrast and coastal geomorphology

³ Department of Physics and Mathematics, University of Alcalá, Alcalá de Henares, Madrid, Spain

⁴ Alfred Wegener Institute for Polar and Marine Research, Am Handelshafen 12, 27568 Bremerhaven, Germany

⁵ Shirshov Institute of Oceanology, Russian Academy of Science, 36 Nahimovskiy prospect, Moscow 117997, Russia

(Bakun et al. 2015). In summer, the typical equatorward atmospheric flow in the EBCS coastal regions, due to the semi-permanent ocean high-pressure systems, is frequently enhanced by the presence of an inland thermal low and by the deflected sea-breezes (Beardsley et al. 1987; Winant et al. 1988; Savijärvi et al. 2005). The alongshore flow often prompts coastal upwelling that intensifies the thermal contrast and feedbacks positively to the coastal-parallel wind. Along EBCS the well-mixed maritime atmospheric boundary layer (MABL) is often confined in the vertical to heights of the order of 1000 m or less, with a capping inversion strengthened by subsiding air, associated primarily to the anticyclone, but also to the descendent branch of the inland thermal low circulation. The aloft subsidence compresses the MABL, that associated to the lowest sea surface temperature (SST) at the coast, forces the onshore tilting of the MABL height. This implies a horizontal temperature gradient across the MABL. Above the MABL inversion layer, and due to the decreasing temperature with height, a thermal wind in opposite direction of the synoptic flow develops. In the inversion layer, a thermal wind in the direction of the synoptic flow develops in association to the increasing temperature with height. This in conjunction with the surface friction and the decreasing wind above the MABL generates a maximum wind speed in the vicinities of the inversion layer which is designated by coastal low-level jet (CLLJ). The strength of the jet is often modulated by the coastal topography and changes in coastal orientation. When the coast turns into the flow partially blocks it, the wind speed is reduced and flow reversal with a hydraulic jump upstream of the cape might develop (Winant et al. 1988). In the opposite case, the flow must turn to follow the coastline thus the thickness of the MABL decreases and the flow accelerates, forming an expansion fan.

The EBCS regions include the California and Humboldt (offshore Chile and Peru) currents in the Pacific Ocean, the west Australia current region in the Indian Ocean and the Canary and Benguela (offshore Namibia and Angola) in the Atlantic Ocean. The offshore EBCS are the major upwelling areas of the global ocean and therefore among the most productive zones, where 17% of the worldwide fish captures take place (Pauly and Christensen 1995). The inland coastal areas along the EBCS are often arid and semi-arid biotopes, identified as highly vulnerable to climate change (Bakun et al. 2010; Snyder et al. 2003). In fact, the evolution of the regional climate and the ecosystems of these regions, in the context of a warming climate, is seen a crucial environmental issue (Bakun et al. 2015; Wang et al. 2015). The first global CLLJ climatology was produced by Ranjha et al. (2013), based on the ERA-Interim reanalysis (Dee et al. 2011), where the presence of persistent coastal jets was identified offshore of the EBCS regions (California, Humboldt, Canary, Benguela and West Australia) and offshore

of Oman, especially in hemispherical summers. Recently, Lima et al. (2017) extended this study using four reanalyses to build a multi-model ensemble mean, for the period 1980–2016, and characterizing in a detailed manner e.g. the seasonal cycle of the different CLLJs systems. Before that Soares et al. (2014, 2018) and Rijo et al. (2017), for the Iberian Peninsula CLLJ and the North African CLLJ, Ranjha et al. (2015) for the Oman CLLJ, and Patricola and Chang (2017) for Benguela had pursued higher resolution dedicated studies. In fact, Ranjha et al. (2013) has shown that along the Canary EBCS two CLLJ exist. They have concluded that the marine wind field along the Canary EBCS is singular, in the sense that the Canary current is disrupted by the influx of denser Mediterranean water into the North Atlantic basin and by the Azores current closer to the surface. But the coast line is also different from other CLLJ areas along EBCS, since its continuity is disrupted by the Gulf of Cadiz, which has an impact on the mean atmospheric flow, giving rise to the existence of two coastal jets: the Iberian Peninsula CLLJ and the Northwest Africa CLLJ.

Ranjha et al. (2013) and Lima et al. (2017) showed that the CLLJs seasonality is stronger in the northern hemisphere than in southern hemisphere. Unlike in California, Iberia and Oman, in the north hemisphere, the North African CLLJ (NACLLJ) occurs all year round, with a lower frequency of occurrence during the boreal winter (December, January, and February; DJF) and with a maximum wind speed further south, when compared to the remaining seasons. Besides the boreal winter (DJF) the remaining seasons are defined as MAM (March, April May, as spring), JJA (June, July, and August, as summer), and SON (September, October November, as autumn). The NACLLJ mean frequency of occurrence is maximum in May, while in California, Iberia and Oman, the highest persistency takes place during the summer months, and are almost inexistent in winter. In the southern hemisphere, the Humboldt and Benguela coastal jets are also present throughout the entire year, with lower frequencies of occurrence in the austral winter (JJA). The Benguela CLLJ was shown to be more persistent in SON, while the Humboldt one in DJF.

Semedo et al. (2016) investigated the impact of climate change on the global CLLJs, identifying important increases in the jet persistency for the Oman and the Iberian CLLJ in summer, and for the NACLLJ in winter. This study was a first attempt to address the evolution of the CLLJs globally, however it was based on two independent low resolution (~ 130 km) simulations performed with the global climate model EC-EARTH. With the goal of investigating the impact of climate warming on the Iberian CLLJ, Cardoso et al. (2016) and Soares et al. (2017a) used higher resolution regional climate simulations, respectively, at 50 and 9 km. These studies revealed consistent future changes on the CLLJ climatology, indicating

an almost doubling of the jet frequency of occurrence in the boreal summer, and also an enlargement of the annual cycle when jets have a significant prevalence, i.e., higher occurrence of the Iberian Peninsula CLLJ from May to September. A higher resolution study on the impact of future global warming on the NACLLJ remained, nevertheless, an open issue.

Recently, Soares et al. (2018) performed the first comprehensive analysis of the NACLLJ in present-climate at high resolution, extending the findings of Ranjha et al. (2013) and Lima et al. (2017). The former paper investigated the NACLLJ main properties, namely its horizontal extension, seasonal cycle of occurrence, and intensity, using a regional climate model hindcast simulation. These simulations were forced at the boundaries with ERA-Interim for the 1980–2012 period and have a 25 km spatial resolution. Soares et al. (2018) exposed the significant occurrence of the jet all-year, with frequencies of occurrence between 20 and 70% in winter and summer, respectively, and around 50% in the intermediate seasons. The NACLLJ extends over broad regions from the offshore areas of north of Morocco to Guineas, and displays positive trends in both the persistency and jet wind speeds for most of the seasons.

The current study is a follow-up of Soares et al. (2018), and using regional climate modelling aims at: evaluating the ability of state-of-the-art regional climate models to represent the surface flow and the low-level coastal wind jets offshore of North Africa, to assess the climate change signal of the surface wind flow over that region, and, finally to study the future properties of the NACLLJ by the end of the twenty-first century.

The regional climate data used correspond to ROM and CORDEX-Africa (Giorgi et al. 2009) simulations. The ROM coupled system builds on, via OASIS coupler, the Regional Atmosphere Model (REMO), the Max Planck Institute Ocean Model (MPIOM), the HAMBURG Ocean Carbon Cycle model (HAMOCC), and the Hydrological Discharge model (HD). All these models are run in a global configuration with the exception of REMO. The ROM acronym follows from REMO–OASIS–MPIOM. The inclusion of explicit atmosphere–ocean feedbacks can substantially influence the spatial and temporal structure of regional climate (Sein et al. 2014, 2015; Cabos et al. 2017). These studies have shown that regional atmosphere–ocean coupled models provide further added value for the simulation of the regional climate, primarily due to a more accurate depiction of the morphological complexity of the land–sea contrasts and relevant mesoscale processes, a better representation of the energy and mass air–sea exchange, and the possibility of a careful choice of the coupling area. Recent studies have shown that ROM can improve the representation of key climatic variables on the regional scale which are not accounted for in the global model MPI-ESM.

Four REMO–OASIS–MPIOM (ROM) regional climate simulations are used: two historical present-climate (1976–2005) and two future climate (2070–2099), in uncoupled and coupled ocean–atmosphere modes. These simulations were forced at the boundaries by the Max-Planck Institute Earth System Model (MPI-ESM) (Giorgetta et al. 2013), and the future runs follow the RCP8.5 greenhouse gases emissions scenario (Riahi et al. 2011). Both simulations cover a wide area that includes Continental Africa and a broad Atlantic Ocean area, at 25 km horizontal resolution in the atmosphere while the ocean component features increased horizontal resolution near North Africa, resulting in a resolution of up to 10 km near the coast. A comprehensive characterization of the NACLLJ present and future properties and corresponding projected anomalies is performed, focusing on its spatial and temporal features, namely the seasonal cycle of the frequency of occurrence, close to surface wind speed (at 10 m height), coastal jet intensity (wind speed at the jet height), jet height (height of the wind speed maxima), as well as the diurnal cycle and inter-annual variability. The NACLLJ is closely linked to the surface flow, therefore an analysis of the ROMs ability to capture the regional surface winds as well as the vertical structure is paramount, particularly in the context of other RCMs. The CORDEX-Africa initiative (Giorgi et al. 2009; Hewitson et al. 2012) constitutes the latest and highest resolution (~50 km) multi-model dataset, at a continental scale, that allows the characterization of the present and future climates in the North African region. Therefore, the present-day climate evaluation of the surface flow and its future assessment is performed jointly using the ROM simulations and the CORDEX-Africa runs.

The paper is organized as follows. In Sect. 2 we introduce the region of study, the observational data, the regional climate simulations and the methods used. An extensive evaluation of the historical simulations, focused on surface wind and vertical profiles, is described in Sect. 3. In Sect. 4 the projected future changes for the NACLLJ are fully characterized. Finally, the most important conclusions are given in Sect. 5.

2 Data and methods

2.1 Regional climate simulations

In the current study, an extensive number of simulations are used to understand the expected future changes on the NACLLJ and also on the related surface wind speeds. Firstly, a set of four simulations are used, including uncoupled and coupled runs for both historical present and future climates: one uncoupled and coupled simulation for the historical period and one uncoupled and coupled simulation for the

future period. These simulations were performed using the ROM model (Sein et al. 2015) in stand-alone atmosphere mode and coupled mode and were forced by historical and RCP 8.5 climate change scenario simulations with the MPI-ESM model carried out in the frame of the CMIP5 project.

The historical simulations span the period between 1950 and 2005, and the future simulations cover the period 2006–2099. All the ROM simulations share the same domain and horizontal resolution (~ 25 km atmosphere), covering the African continent and a large part of the Atlantic Ocean (Fig. 1a). In the vertical, the model has 31 hybrid levels, and temperature and wind components are available every 3 h. The MPIOM configuration differs from that of MPI-ESM. It has a higher horizontal resolution within the coupled domain

spanning from 7 to 25 km near the West African coasts and equatorial Atlantic to 60–65 km at 45°S (Fig. 1b). It comprises 40 z-coordinate vertical levels. These simulations were used in a number of evaluation studies regarding decadal predictions of West African monsoon rainfall (Paxian et al. 2016; Paeth et al. 2017) and the impact of South Atlantic Anticyclone in the generation of coupled model biases in the Angola-Benguela frontal zone (Cabos et al. 2017).

A set of CORDEX-Africa runs is also used, to assess the relative performance of the ROM simulations to represent the NACLJ offshore surface flow in the historical runs; and understand how the surface flow is projected to change in the North African CLLJ region in response to global warming. The CORDEX-Africa dataset (<http://esg-dn1.nsc.liu.se/>

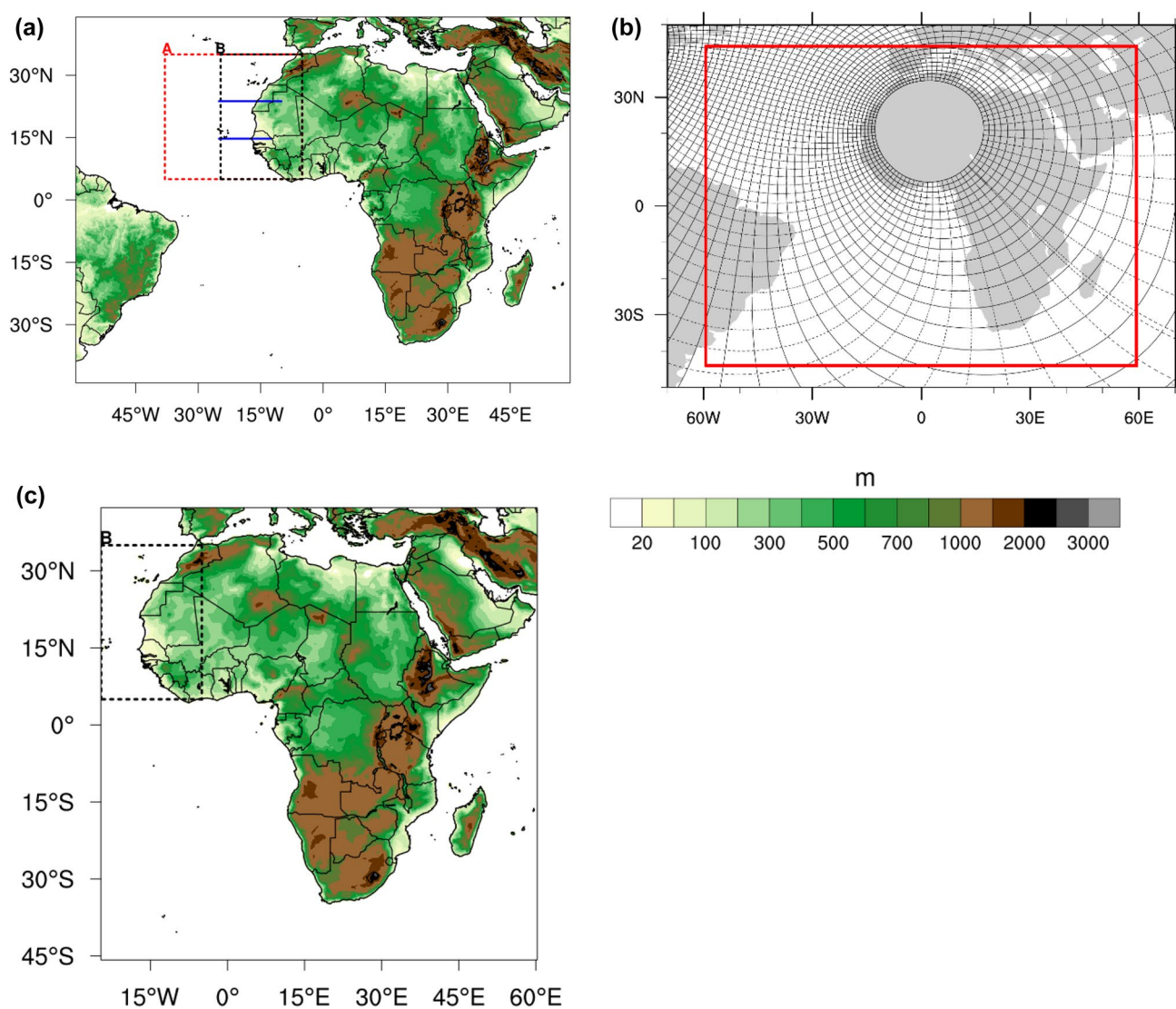


Fig. 1 a ROM simulation domain (full map area), b MPIOM horizontal grid and c CORDEX-Africa common domain (full map area). The dashed red and black lines delimit the areas of analysis regarding

the North African coastal low level jet and model evaluations, respectively. The blue lines mark two representative cross-sections

[esgf-web-fe/live](#)) provides surface variables, and the first pressure level at 850 hPa, way higher than the typical height of jet occurrence. This data is available at daily time scale, covering the African continent (Fig. 1c) at 0.44° resolution. In this study, 20 CORDEX-Africa simulations are included (Table 1), covering present (historical) and future simulations, in agreement with the RCP8.5 emission scenario (Riahi et al. 2011), for 1976–2005 and 2070–2099 periods, respectively.

2.2 Observations

To perform an evaluation of the surface variables as represented by the historical simulations from the regional climate models (RCMs), two types of observational datasets were considered: the Cross-Calibrated Multi-Platform (CCMP, Atlas et al. 2011) surface wind fields and the National Oceanic and Atmospheric Administration (NOAA) SST fields (Reynolds et al. 2007). These two datasets were used to evaluate the surface wind speed at 10 m and the SSTs field, respectively.

The CCMP data set was developed by NASA (National Aeronautics and Space Administration), combining cross-calibrated satellite winds, from microwave satellite instruments, in situ wind measurements, and European Centre for Medium-Range Weather Forecasts (ECMWF) reanalysis, using a variational analysis method. The CCMP has 0.258° of horizontal resolution and is provided at 6-hourly

frequency. The output spans the period from July 1987 to June 2011, without gaps.

The NOAA Optimum Interpolation Sea Surface Temperature, V2 high resolution data set combine ocean temperature satellite and in situ observations, and model analysis (Reynolds et al. 2007). The daily SST fields have a $0.25^\circ \times 0.25^\circ$ spatial resolution, and ranges from September 1981 to the present time.

Aiming at the evaluation of the vertical atmospheric structure given by the ROM runs, all the available radiosondes within the domain were collected. In Figure S1 the locations of the seven radiosondes, with wind or/and temperature data, are displayed, and in Table S1 the number of missing values for each of the variables is listed. Unfortunately, it is fair to acknowledge the scarcity of 3D observational data in the region of interest. This scarcity is even larger when offshore vertical atmospheric information and sub-daily temporal data is needed, which is the case to assess the jet features. Since the historical runs are not synchronized with observations, any comparison has to have a statistical climatological character, which recommends significant observational sampling.

Finally, in an attempt to add robustness to the vertical profiles assessment the 3D temperature and wind ERA-Interim data were retrieved and compared with the ROM results. However, we should keep in mind the different resolutions of ROM (~ 25 km) and ERA-Interim (~ 80 km).

Table 1 CORDEX-Africa regional climate models considered in the present study, along with the respective forcing global climate model, and the acronym for each model combination (RCM-GCM)

Global climate model (forcing models)	CORDEX-Africa regional climate model	Acronym	Institution	References
ICHEC-EC-EARTH	CCLM4-8-17	CLM1	Climate Limited-area Modelling Community	Rockel et al. (2008)
MOHC-HadGEM2-ES		CLM2		
CNRM-CERFACS-CNRM-CM5		CLM3		
MPI-M-MPI-ESM-LR		CLM4		
ICHEC-EC-EARTH	HIRHAM5	DMI	Danish Meteorological Institute	Christensen et al. (2007)
ICHEC-EC-EARTH	RACMO22E	KNMI1	Koninklijk Nederlands Meteorologisch Instituut	Van Meijgaard et al. (2008)
MOHC-HadGEM2-ES		KNMI2		
ICHEC-EC-EARTH	REMO2009	MPI1	Helmholtz-Zentrum Geesthacht, Climate Service Center, Max Planck Institute for Meteorology	Jacob et al. (2001)
MPI-M-MPI-ESM-LR		MPI2		
ICHEC-EC-EARTH	RCA4	SMHI1	Swedish Meteorological and Hydrological Institute	Samuelsson et al. (2011)
MOHC-HadGEM2-ES		SMHI2		
CNRM-CERFACS-CNRM-CM5		SMHI3		
MPI-M-MPI-ESM-LR		SMHI4		
IPSL-IPSL-CM5A-MR		SMHI5		
CCCma-CanESM2		SMHI6		
CSIRO-QCCCE-CSIRO-Mk3-6-0		SMHI7		
MIROC-MIROC5		SMHI8		
NCC-NorESM1-M		SMHI9		
NOAA-GFDL-GFDL-ESM2M		SMHI10		

All models at 0.44° resolution

2.3 Evaluation methods and ensemble mean building

Climate change assessment studies should encompass a thorough evaluation of the historical period simulation results at their base. The surface wind speeds at 10 m height from the historical simulations, from both ROMs and the set of CORDEX-Africa runs, are compared against the CCMP wind speeds. The RCM runs and the CCMP data sets have different horizontal resolutions. Therefore, the ROM simulations were interpolated to the 0.25° CCMP grid using the nearest neighbour grid point. The CCMP and the CORDEX-Africa RCMs were interpolated to a common regular non-rotated grid at 0.44°, using the same interpolation method. In this way, a measure of the ROM’s performance is done at 25 km, keeping the extra features offered by the ROM’s higher resolution, which are vital for studying the coastal low-level jets. Furthermore, a completely fair evaluation of all the models is done at the 0.44° grid of the CORDEX-Africa, interpolating additionally the ROM results to this grid, and thus offering a clear idea of the relative model’s performance.

The ROMs historical period simulations SST fields were also evaluated against the NOAA SST dataset, and were interpolated to the observed SST grid conservatively (Suklitsch et al. 2008). The interpolations were performed using the Climate Data Operators (CDO user’s guide: Schulzweida et al. 2006) functions *remapnn* and *remapcon*. In order to evaluate each model performance in the reproduction of the historical climate, wind speed at 10 m from ROM and CORDEX-Africa, as well as SST from ROM were compared against the observational datasets. As in Soares et al. (2012, 2017b) and Cardoso et al. (2013, 2018), bias, percentage bias, mean absolute error (MAE), mean absolute percentage error (MAPE), root mean square error (RMSE), normalized standard deviation, spatial correlation (Wilks 2006) and Willmott-D score (Willmott et al. 2012) were computed for all the available points and time scales (monthly, seasonally and yearly). The Willmott-D score is defined as,

$$D = \begin{cases} 1 - \frac{\sum_{k=1}^N |p_k - o_k|}{2 \sum_{k=1}^N |o_k - \bar{o}|}, & \text{if } \sum_{k=1}^N |p_k - o_k| \leq 2 \sum_{k=1}^N |o_k - \bar{o}| \\ \frac{2 \sum_{k=1}^N |o_k - \bar{o}|}{\sum_{k=1}^N |p_k - o_k|} - 1, & \text{if } 2 \sum_{k=1}^N |o_k - \bar{o}| < \sum_{k=1}^N |p_k - o_k|, \end{cases} \quad (1)$$

where o_k represents the observed values, p_k the modelled values, \bar{o} the mean of observed values, \bar{p} the mean of modelled values and N the number of observed/modelled events. For the Willmott D score (Willmott et al. 2012), a perfect skill is obtained when $D = 1$, while no skill gives $D = -1$. With this metric, not only differences in the mean but also differences in the standard deviation are assessed. The

probability distribution functions (PDFs) were analysed with the Yule-Kendall skewness measure (Ferro et al. 2005) and PDF matching skill scores (S ; Boberg et al. 2009). The PDFs are built by putting the surface wind data into bins of 1 ms^{-1} width starting at 0 ms^{-1} , and afterwards each bin’s frequency is computed:

$$YK = \left[\frac{(P_{95} - P_{50}) - (P_{50} - P_5)}{(P_{95} - P_5)} \right]_{model} - \left[\frac{(P_{95} - P_{50}) - (P_{50} - P_5)}{(P_{95} - P_5)} \right]_{obs}, \quad (2)$$

$$S = \sum_1^N \min(E_M, E_O), \quad (3)$$

where P represents the percentiles, E_O the empirical distribution function of observed near surface wind speed, E_M the model’s counterpart, 1 and N refer to the surface wind speed bins. The first score indicates the difference between the modelled and observed PDF skewness, thus close to zero values indicate a good match between the PDFs shape. The second score provides an integral measure of the overlap between the observed and modelled PDFs, i.e. the common PDF area. $S = 1$ or 100% indicates a perfect overlap.

With the aim of better assessing the projected changes on the surface wind speeds and reduce model uncertainty, a ranking of the CORDEX-Africa RCMs based on the present-climate evaluation is performed (Christensen et al. 2010). With this ranking, a weight is ascribed to each individual model and multi-model ensemble mean is computed. By assigning greater weights to higher ranking models it is assumed that uncertainty of the projections is reduced (Christensen et al. 2010; Nogueira et al. 2018). Following Soares et al. (2015, 2017c) and Cardoso et al. (2016), for each metric, the individual model ranks are normalized so that they can be compared. Firstly the individual model ranks should be positive. Thus, for the metrics in which the best expected result is zero (bias, MAE and RMSE), the inverse of its absolute value was calculated. Since D-Willmott and correlation are bounded between -1 and $+1$, it is shifted one unit by adding $+1$ to their values before the rank computation. For normalized standard deviation, the best expected value is 1, so this metric was transformed as,

$$\vartheta_n = \begin{cases} \sigma_n & \text{if } \sigma_n < 1 \\ \frac{1}{\sigma_n} & \text{if } \sigma_n > 1. \end{cases} \quad (4)$$

Similarly, the Yule–Kendall becomes:

$$YK_{new} = \begin{cases} YK + 1 & \text{if } YK < 0 \\ \frac{1}{YK+1} & \text{if } YK > 0. \end{cases} \quad (5)$$

The S score is not changed. The individual models ranks, for each metric, were then obtained by dividing each value by the sum of all values from all the models, being the sum of the ranks equal to 1. Weights were then calculated, by multiplying the ranks of all the metrics. Finally, each weight is divided by the sum of the weights so that the sum of the weights is equal to 1. Since some of the metrics evaluate similar characteristics, the percent bias and mean absolute percentage error were not considered in the weights design. The near surface wind speed daily values of the multi-model ensemble mean were obtained as,

$$sfcWind = \frac{\sum_{i=1}^N sfcWind_i w_i}{\sum_{i=1}^N w_i}, \tag{6}$$

where $sfcWind_i$ is the daily surface wind speed at 10 m height, w_i is the weight of each model and N is the number of models. The CORDEX-Africa ensemble PDF was obtained as:

$$PDF(sfcWind) = \sum_{i=1}^N PDF(sfcWind)_i w_i. \tag{7}$$

Finally, the wind and temperature profiles from the ROM simulations are compared against the radiosondes, at 00 and 12UTC, and ERA-interim, at a 6-hourly sampling, computing the bias, MAE, MAPE (only for wind) and RMSE, for the mean climatological Julian days.

2.4 Coastal low level jet analysis

The full set of ROM simulations, specifically the wind and temperature vertical profiles, are automatically inspected to

detect the presence of a CLLJ, at a grid point level every 3 h. The CLLJ identification is based on the filtering algorithm proposed by Ranjha et al. (2013), later revised by Lima et al. (2017). The algorithm is based on the analysis of the vertical wind speed and temperature profiles (details are reported in the referred studies). The set of NACLJ occurrences enables the characterization of the coastal jet properties in present (1976–2005) and in future (2070–2099) climates, for one greenhouse gases emission scenario (RCP 8.5). Additionally, the projected changes of surface wind speed at 10 m height, including the ROM and the multi-model ensemble mean of CORDEX-Africa simulations, are also analyzed.

3 Evaluation of the historical simulations

3.1 SST, surface wind and atmospheric vertical structure

Figure 2 and Table 2 show the surface wind speed errors for all the historical runs (ROM uncoupled and coupled as well as individual CORDEX-Africa RCMs and multi-model ensemble mean) from the comparison with the CCMP observational dataset. The evaluation is performed for the area delimited by the black dashed line in Fig. 1a. Table 2 includes, besides the Yule-Kendall skewness measure and the S score, the mean bias, the mean absolute percentage error, the normalized standard deviation, the Wilmott-D and the yearly spatial correlation coefficient. Since the historical runs are not synchronized in time with the observations, the validation metrics correspond to seasonal mean values, with the exception of the S and Yule–Kendall skill scores, which compare daily PDFs, and yearly spatial correlation coefficient. In general, the error values depict good performance

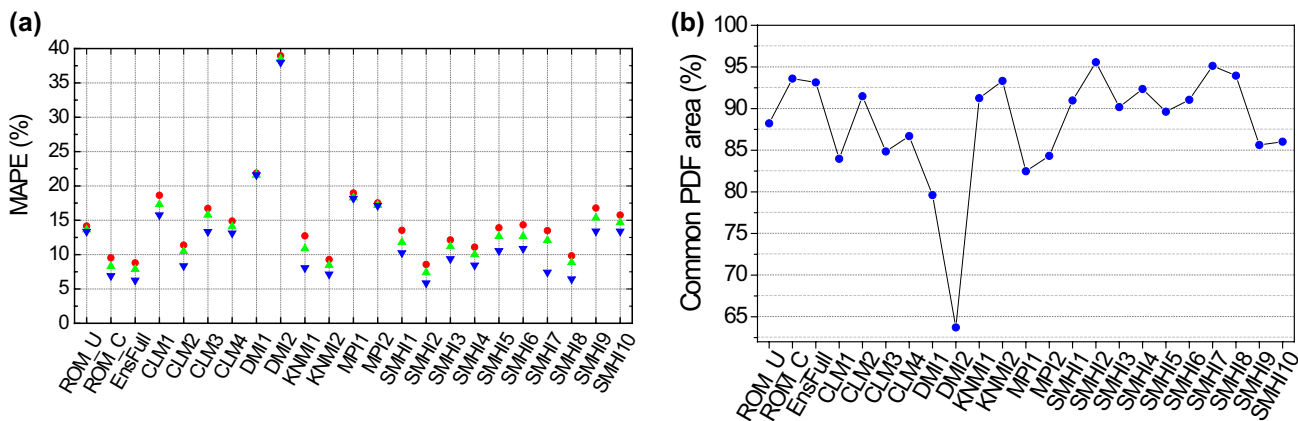


Fig. 2 ROM simulations (U-uncoupled, C-coupled), CORDEX-Africa individual runs and multi-model ensemble mean (EnsFull) near surface wind errors compared to CCMP winds, pooling together all the grid points of the area delimited in dashed black in Fig. 1.

The validation metrics are **a** the MAPE and **b** S. For the MAPE the errors are computed for different time periods of near surface wind (monthly in red, seasonally in green and yearly in blue), pooling all data together

Table 2 ROM and CORDEX-Africa individual RCM statistical errors and skill scores

RCMs	Bias (m/s)	MAPE (%)	Normalized Standard Deviation	Wilmott-D	Spatial Correlations	S	Yule–Kendall
0.25°							
ROM Uncoupled	0.82	13.63	0.83	0.60	0.96	88.22	– 0.004
ROM Coupled	0.41	8.30	0.99	0.76	0.97	93.60	0.004
0.44°							
ROM uncoupled	0.82	13.60	0.83	0.60	0.96	88.42	– 0.002
ROM coupled	0.41	8.27	0.99	0.76	0.97	93.88	0.004
CLM1	0.97	17.69	1.17	0.50	0.96	83.96	– 0.001
CLM2	0.41	10.47	1.14	0.71	0.93	91.48	– 0.045
CLM3	0.82	16.50	1.11	0.54	0.95	84.85	0.041
CLM4	0.80	14.32	1.03	0.59	0.95	86.70	0.012
DMI1	1.33	21.88	1.01	0.38	0.96	79.61	– 0.036
DMI2	2.34	38.54	1.29	– 0.09	0.80	63.72	– 0.098
KNMI1	0.33	10.78	1.29	0.68	0.96	91.25	– 0.035
KNMI2	0.30	8.36	1.27	0.76	0.96	93.32	– 0.006
MPI1	1.12	18.76	0.91	0.47	0.93	82.47	– 0.031
MPI2	1.05	17.18	0.85	0.50	0.93	84.32	– 0.017
SMHI1	0.33	12.08	1.30	0.65	0.92	90.97	– 0.013
SMHI2	0.25	7.61	1.14	0.79	0.95	95.57	0.014
SMHI3	0.21	11.20	1.32	0.67	0.94	90.18	0.035
SMHI4	0.33	10.07	1.21	0.70	0.95	92.34	0.012
SMHI5	0.60	12.49	1.28	0.63	0.93	89.62	– 0.022
SMHI6	0.35	12.58	1.41	0.63	0.94	91.05	– 0.021
SMHI7	0.24	12.17	1.00	0.64	0.87	95.12	0.007
SMHI8	0.35	9.03	1.10	0.74	0.95	93.95	– 0.016
SMHI9	0.72	15.40	1.44	0.55	0.93	85.63	– 0.061
SMHI10	0.82	14.71	1.21	0.57	0.96	86.02	– 0.029
EnsFull	0.33	7.88	1.12	0.77	0.98	93.14	– 0.028

These enabled the ranking of the CORDEX-Africa RCMs and the building of the multi-model ensemble mean. The model errors that were computed considering the CCMP surface wind dataset as reference are: seasonal bias, MAPE, Normalized Standard deviation and Wilmott-D score, the yearly spatial correlation, daily S pdf matching skill score and Yule–Kendall score. All errors were computed pooling all grid boxes together

of the RCMs, although revealing some spread in the evaluation metrics (Table 2). The bias, where error compensation may exist, show a generalized overestimation of surface wind speed that can escalate by more than 10x, from ~ 0.2 to ~ 2.3 m/s. However, the majority of RCMs has bias values lower than 1 m/s. More importantly, the MAPEs are in the range of ~ 7 . to $\sim 20\%$, with an isolated value of $\sim 40\%$ (Fig. 2a). The seasonal-spatial variability, here measured by the normalized standard deviation, reveals that models tend to overestimate the variability, however, a few represent it well with values around 1, like the ROM coupled simulation, DMI1, SMHI7 and CLM4. The spatial correlations are quite high, higher than 0.90 in almost all models. The quality of the wind speed distributions is summarized by the S score and the Yule–Kendall metric. Largely, the S scores are larger than 80% showing that RCM PDFs overlap by more than 80% (Fig. 2b). The low Yule–Kendall values support the

good agreement between the probability distributions and the similarity in the PDF's skewness. Overall, it can be seen that the ROM coupled simulation presents the best performance in reproducing the present-day climate, near surface wind speed offshore Northwest Africa, compared to the remaining RCM simulations. Among the CORDEX-Africa set of simulations, the SMHI2 displays the lowest errors. The CORDEX-Africa multi-model ensemble mean outperforms most of the individual models (last row in Table 2). Finally, the errors in the ROM simulations are similar when considering the CCMP dataset at 25 km and 0.44°, revealing, on the one hand, the ROM added details given by the higher resolution, and, on the other hand, that these ROM simulations rank as one of the best performing when directly compared with CORDEX-Africa.

The seasonal mean surface wind speeds for present-climate (historical simulation results), given by both

ROM (uncoupled and coupled) simulations and the CORDEX-Africa multi-model ensemble mean (EnsFull) are depicted in Fig. 3, along with the respective CCMP seasonal means observational counterparts. A qualitative inspection reveals that the seasonal wind speed patterns are rather analogous, as expected by the high values of spatial correlations aforementioned. Moreover, a slight overestimation is clear in most seasons, especially near

the coast, islands and the NACLLJ areas (Soares et al. 2018). These higher model wind speed values near the coast may be linked to the known deficiencies that CCMP dataset presents in those regions, due to backscatter from land, which contaminates the wind speed measurements (Tang et al. 2004). In summer, the inability of the uncoupled run to represent the lower wind speeds around 10°N, is noticeable. The ROM coupled simulation has the lowest

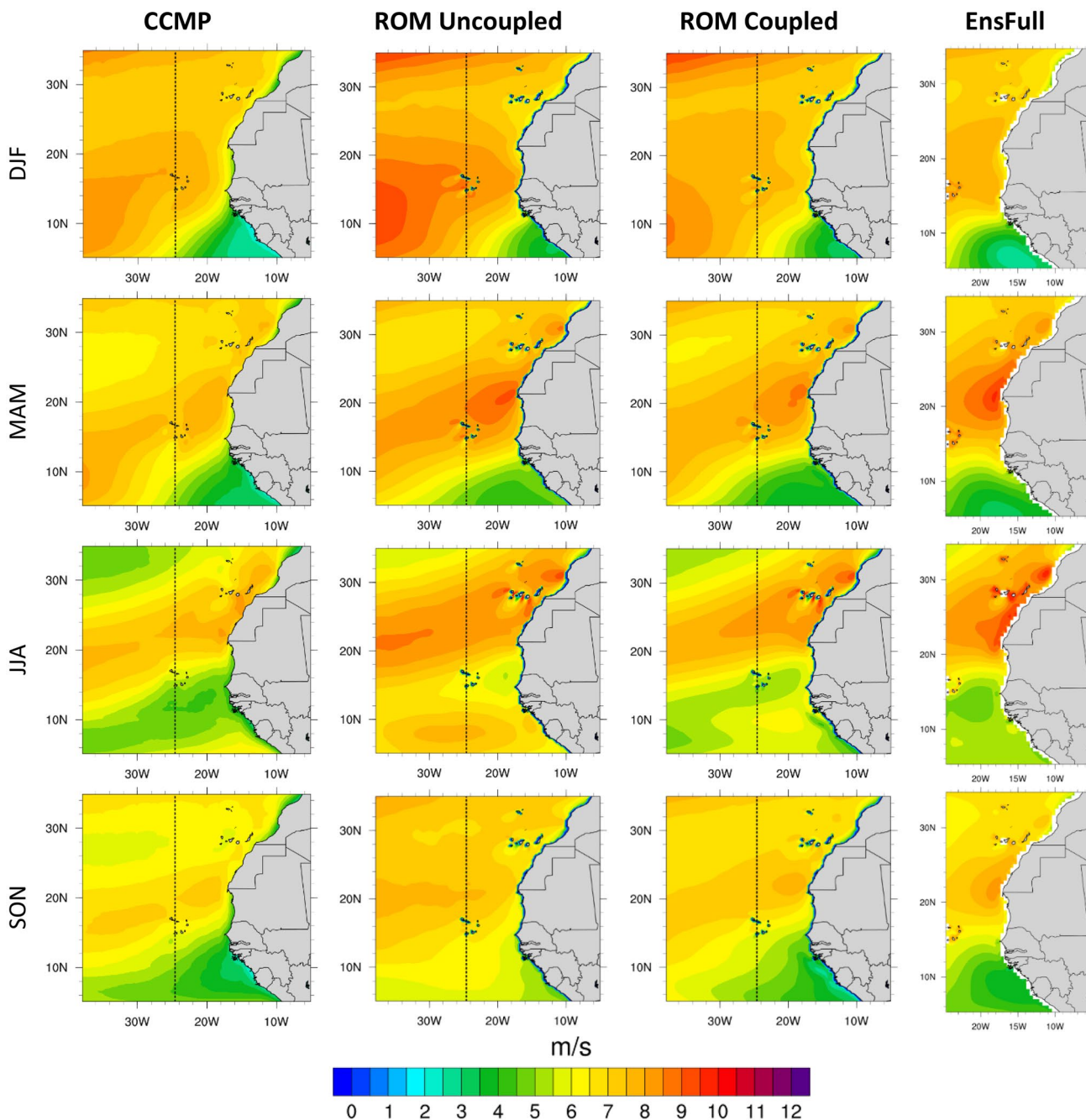


Fig. 3 Seasonal mean surface wind speed (at 10 m) from the CCMP observational dataset, and from the historical ROM simulations (coupled and uncoupled) and CORDEX-Africa full multi-model ensemble

mean (EnsFull), for 1976–2005 period. Dotted line represents the left limit of the CORDEX-Africa full multi-model ensemble (EnsFull) domain

surface wind speeds, while the CORDEX-Africa multi-model ensemble mean exhibits the highest surface winds. These maxima are associated to flow around capes or to the Canary islands wakes.

The comparison between the ROM and the radiosondes' wind and temperature profiles shows in general a good model ability to represent qualitatively the vertical structure of the atmosphere in the CLLJ region (Table S2 and Figure S2). It should be emphasized the number of missing values (Table S1) that are clearly responsible for the largest discrepancies between model and observations. Note that for the two radiosondes with the largest amount of data available, Dakar and Santa Cruz the missing values are around 70%.

ERA-Interim offers a much better resource for evaluating the atmospheric vertical structure. Table S3 depicts the computed errors and Figure S3 shows the climatological profiles, with 6-hourly sampling, of the ROM simulations along with ERA-Interim. Overall, for the two points analyzed (P1 and P2) the wind and temperature MAEs are ~ 1.4 m/s and ~ 1.2 °C, respectively, for the full diurnal cycle (Table S3). The vertical mean profiles of ROM are rather similar with the ones of ERA-Interim (Figure S3), except for some overestimation of the wind speed by the ROM simulations. Yet, this is probably due to the higher ROM resolution and the improved ability to represent the near coastal flow.

With regards to the ROMs ability to represent the regional pattern of SST, Table 3 exhibits error measures comparing the SSTs simulated by ROM against the NOAA dataset. The simulations show good and comparable skills in describing the regional SSTs. The better quality is dependent on the selected error. Overall, it seems that the ROM uncoupled simulation describes in an improved way SST since has lower errors. A common trait of regional coupled models is to reproduce colder SSTs than the forcing global models (Li et al. 2012). The ROM uncoupled simulation shows an SST bias of -0.26 °C and the coupled -0.65 °C, and the MAEs are 0.63 °C and 0.85 °C, respectively. However, e.g. the normalized standard deviation (S score) given by the coupled simulation is much closer to 1 (100%) than the uncoupled simulation counterpart.

3.2 North African coastal low-level jet

The NACLLJ present-climate seasonal cycle in the ROM (uncoupled and coupled) simulations, is depicted in Fig. 4. The frequencies of jet occurrence show that the coastal jet emerges all year and that the uncoupled and coupled simulations give rather similar seasonal jet patterns. In winter, the NACLLJ is clearly present, unlike the Iberian jet (Soares et al. 2017b; Cardoso et al. 2016), with frequencies of occurrence above 10% in the coastal regions between the Western Sahara and Senegal. This agrees with the regional climate hindcast results reported by Soares et al. (2018). The jet persistency increases in spring, reaching frequencies of occurrence above 40% in two local maxima, in the vicinities of two sharp coastal features, the Ras Nouadhibou Peninsula and Cape Vert (Dakar). In summer, the two maxima appear further north, one downwind Cape Ghir and the second in the central part of the offshore areas of Western Sahara (downwind of the Canary isles and Cape Bojador). These maxima show a persistency over 40% and 60%, respectively, in the uncoupled ROM simulation. In the case of the coupled simulation the summer maxima are even higher, reaching more than 70% of jet frequency in the southern maximum. Finally, in autumn the frequencies of occurrence are still relevant with a single maximum value around 40% near the southern Western Sahara south of cape Bojador, in both coupled and uncoupled runs. Interestingly, the offshore areas where the jet is more persistent are horizontally more extended in the case of the uncoupled simulation. In fact, for the coupled simulations those areas are more confined and localized in narrow coastal regions. This is in accordance with the areas with minimum SSTs, especially for summer and autumn. The SST resolution in the coupled simulation is higher than in the uncoupled. Thus, in the latter, the coastal areas with the lowest SST are larger, whilst in the coupled simulations these minima are thin stripes along the coast (not shown). The upwelling signal in the coupled simulation is not only confined to thinner bands, but it is also stronger, hence the stronger jets in these simulations. Lastly, the historical seasonal frequencies of occurrence greatly resemble the frequencies shown in Soares et al. (2018) for present-climate, based on a ROM hindcast run forced by ERA-Interim.

Table 3 ROM Uncoupled and Coupled SST statistical errors and skill scores using the NOAA database as reference

RCMs	Bias (°C)	MAE (°C)	Normalized Standard Deviation	Wilmott-D	Spatial Correlation	S	Yule-Kendall
ROM uncoupled	-0.26	0.63	1.10	0.87	0.99	88.65	-0.049
ROM coupled	-0.65	0.85	0.99	0.82	0.97	93.21	0.074

The errors are: seasonal bias, MAE, Normalized Standard Deviation and Wilmott-D score, the yearly spatial correlation and daily S pdf matching skill score and Yule-Kendall score. All errors were computed pooling all grid boxes together

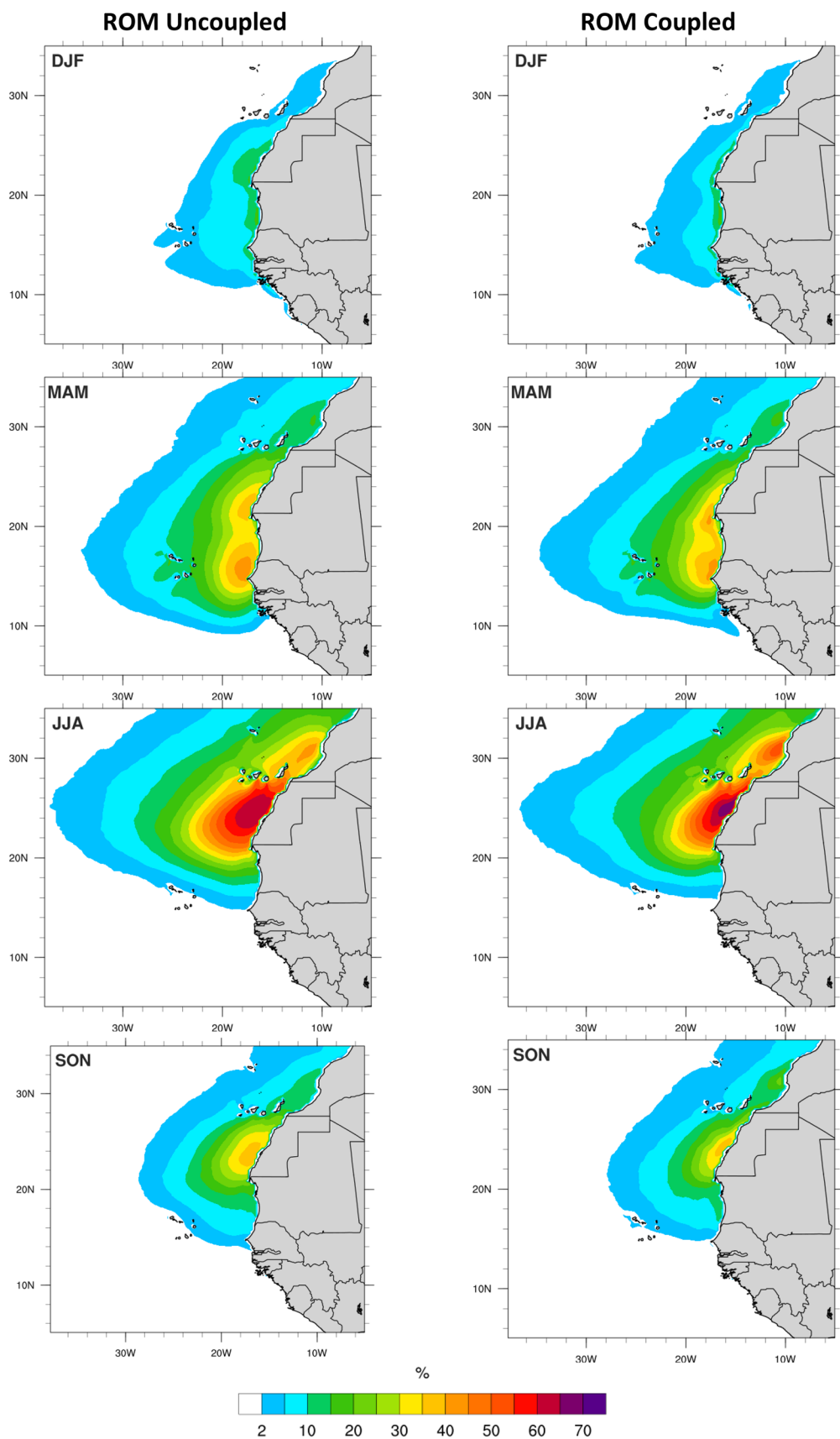


Fig. 4 Seasonal frequency of occurrence of the coastal low-level jet from the uncoupled and coupled ROM historical (1976–2005) simulations

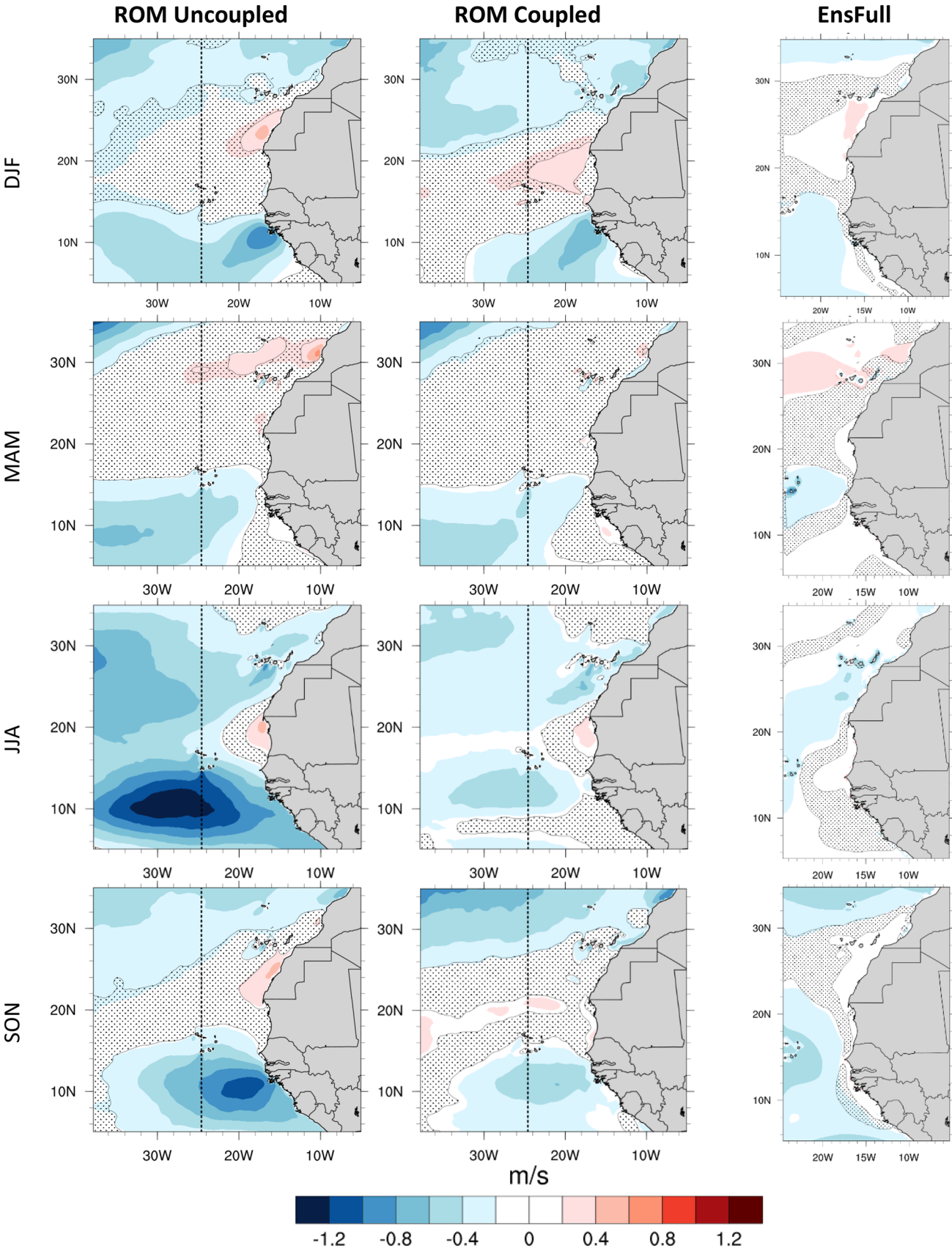


Fig. 5 Delta change of seasonal mean wind speed at the surface, future minus present (2070–2099 minus 1976–2005), from the ROM simulations (uncoupled and coupled) and the CORDEX-Africa full multi-model ensemble mean. Shaded areas specify changes not statistically significant using a Student's *t* test at the 90% confidence level

4 The future of the North African offshore surface wind and coastal low-level jet

4.1 Surface wind speed

A close inspection of the differences between future and historical surface wind speeds (Fig. 5), reveals that, at seasonal scale, the ROM simulations project qualitatively similar changes to the CORDEX-Africa multi-model ensemble mean. Yet, in some locations ROMs variations are stronger, particularly in the uncoupled simulation. The spatial pattern of the surface wind speed delta change is rather heterogeneous, especially for the case of the higher resolution ROMs runs. In future climate, the ROM simulations indicate that, in all seasons, surface wind speed is projected to increase in coastal offshore areas where the coastal jet occurs; nonetheless, these positive differences are small (< 0.5 m/s). Examples of this significant increase are the offshore areas of Western Sahara in winter, and the areas offshore Agadir in Morocco in spring. This is not unexpected as, in these areas the land-sea contrast is enhanced in the future. The future SST rise is projected to be smaller than the temperature escalation over land (not shown). The ROM runs also project a decrease further offshore regions of the Guineas (Guinea Bissau and Guinea Conakry). This decrease is larger for the ROM uncoupled simulation and can reach noteworthy values above 1 m/s in summer and autumn. Furthermore, in summer, the projected surface wind speed decrease extends to vast offshore areas. The CORDEX-Africa ensemble mean also projects wind speed decreases, with some geographical differences and with values of wind speed change lower than 0.6 m/s.

Figure 6 shows PDFs of the seasonal wind speed at the surface from the uncoupled and coupled ROM runs, and the CORDEX-Africa multi-model ensemble mean, for present and future climates. For the full common domain analyzed, the three projections point out to a slight shift towards lower surface wind speeds in the future, and a correspondent decrease in the highest wind speeds, more noticeable in autumn, winter and summer. In spring, the future changes are negligible. The projected changes are more visible in the ROM simulations. This is in agreement with Fig. 5 above, in spite of the local increases within the NACLLJ areas.

The near surface wind speed projected changes and its spread according to the RCP8.5 emissions scenario are detailed in Table 4 and Fig. 7. Table 4 reveals that the ROM simulations and the CORDEX-Africa multi-model ensemble

mean project a generalized decrease of the seasonal mean surface wind speeds within the NACLLJ region, except for a small increase (0.03 m/s; $< 1\%$ in Fig. 7) in spring for the CORDEX-Africa multi-model ensemble mean. The projected reductions are more noticeable in the case of the uncoupled and coupled ROM simulations, in the range of -8 and -2% in summer and spring, respectively. In autumn the future results project a decrease of seasonal mean wind speed at the surface of around 4%, compared to the historical runs. Regarding inter-annual variability, Table 4 shows, as expected, much more variability linked to the ROM simulations, since the multi-model ensemble mean merges different non-synchronous runs, which end up flattening, to a certain extent, the inter-annual variability. Interestingly, the inter-annual standard deviations of the seasonal near surface winds is projected to increase importantly in winter and summer, for the ROM runs, and decrease notably in spring and in a smaller extent in autumn. The multi-model ensemble mean points out to quite different changes in the inter-annual variability: no changes in winter, small increases in spring and significant decreases in summer and in autumn.

Figure 7 shows the seasonal mean surface wind speed delta changes between the future and the historical simulations, averaged over the full common domain, and for the ROM runs, the individual CORDEX-Africa RCMs and the CORDEX-Africa multi-model ensemble mean. Looking at Fig. 7 a large spread between the ensemble individual members is visible for all seasons. The majority of the RCMs concurs with a clear decrease of the seasonal mean near surface wind in winter, summer and autumn and an increase in spring. In winter, the ROM runs and the CORDEX-Africa multi-model ensemble mean project a small decrease of near surface wind, in the range of -2 and -4% , but the individual models show changes between $+6$ and -10% .

4.2 North African coastal low-level jet

The intra-annual cycle of the NACLLJ jet mean wind speed (wind speed at the jet height) and coastal jet mean frequency of occurrence for the region of interest (spatial average for the area; see Fig. 1) and for present and projected future climates, are introduced in Fig. 8. Overall, both uncoupled and coupled ROM simulations reveal an important increase in the jet occurrence for all months, especially in February, March, June and November (around 4.7%, 4%, 3.7%, and 5.6%, respectively). These increases are roughly similar and consistent for the ROM simulations throughout the annual cycle. Regarding the jet mean wind speed, the estimated future changes are more noticeable in November and December and then from February to May. These changes correspond to higher mean wind speeds for the referred months, in the range of 5–12% (highest in November). From June to October the future changes are quite negligible.

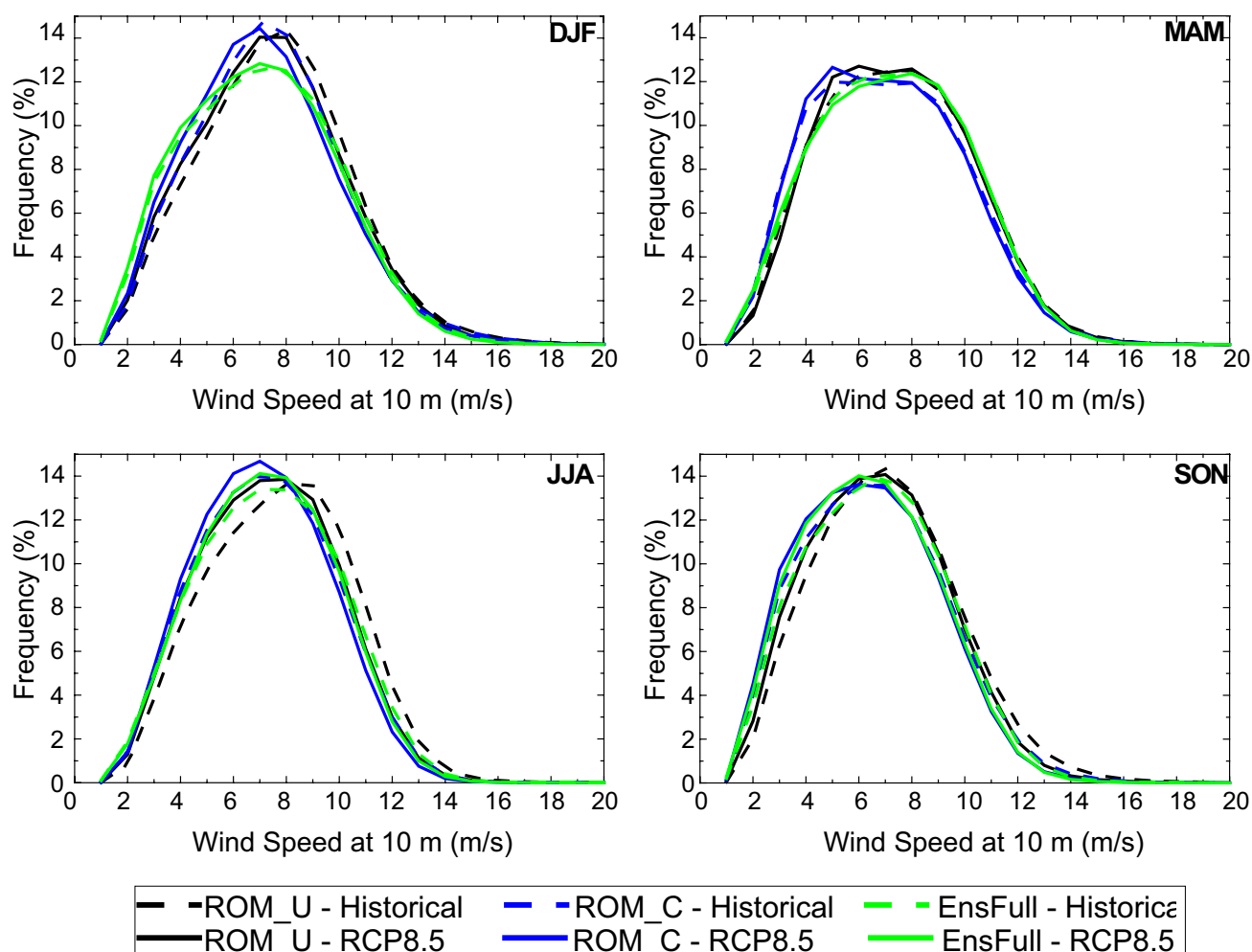


Fig. 6 Seasonal PDFs of wind speed at the surface (10 m height) from the ROM simulations (*U* uncoupled, *C* coupled) and from the CORDEX-Africa full multi-model ensemble mean. Results from the historical and future simulations

Table 4 Mean and inter-annual standard deviation of seasonal near surface wind speed (at 10 m; seasonal mean for the area of interest B marked in Fig. 1b)

	DJF		MAM		JJA		SON	
	Mean	Std	Mean	Std	Mean	Std	Mean	Std
ROM_U								
Historical	7.10	0.27	6.93	0.31	7.28	0.26	6.59	0.26
Future	6.86	0.35	6.92	0.19	6.83	0.34	6.25	0.25
Relative difference (%)	-3.50	29.63	-0.14	-38.71	-6.18	30.77	-5.16	-3.85
ROM_C								
Historical	6.83	0.26	6.60	0.31	6.75	0.19	6.09	0.22
Future	6.59	0.37	6.55	0.21	6.58	0.21	5.86	0.19
Relative difference (%)	-3.51	42.31	-0.76	-32.26	-2.52	10.53	-3.78	-13.64
EnsFull								
Historical	6.54	0.13	6.77	0.13	6.80	0.08	6.10	0.10
Future	6.41	0.13	6.80	0.14	6.70	0.07	5.87	0.07
Relative difference (%)	-1.99	0	0.44	7.69	-1.47	-12.50	-3.77	-30.00

Results given by the ROM simulations (uncoupled and coupled) and the CORDEX-Africa full multi-model ensemble mean (EnsFull)

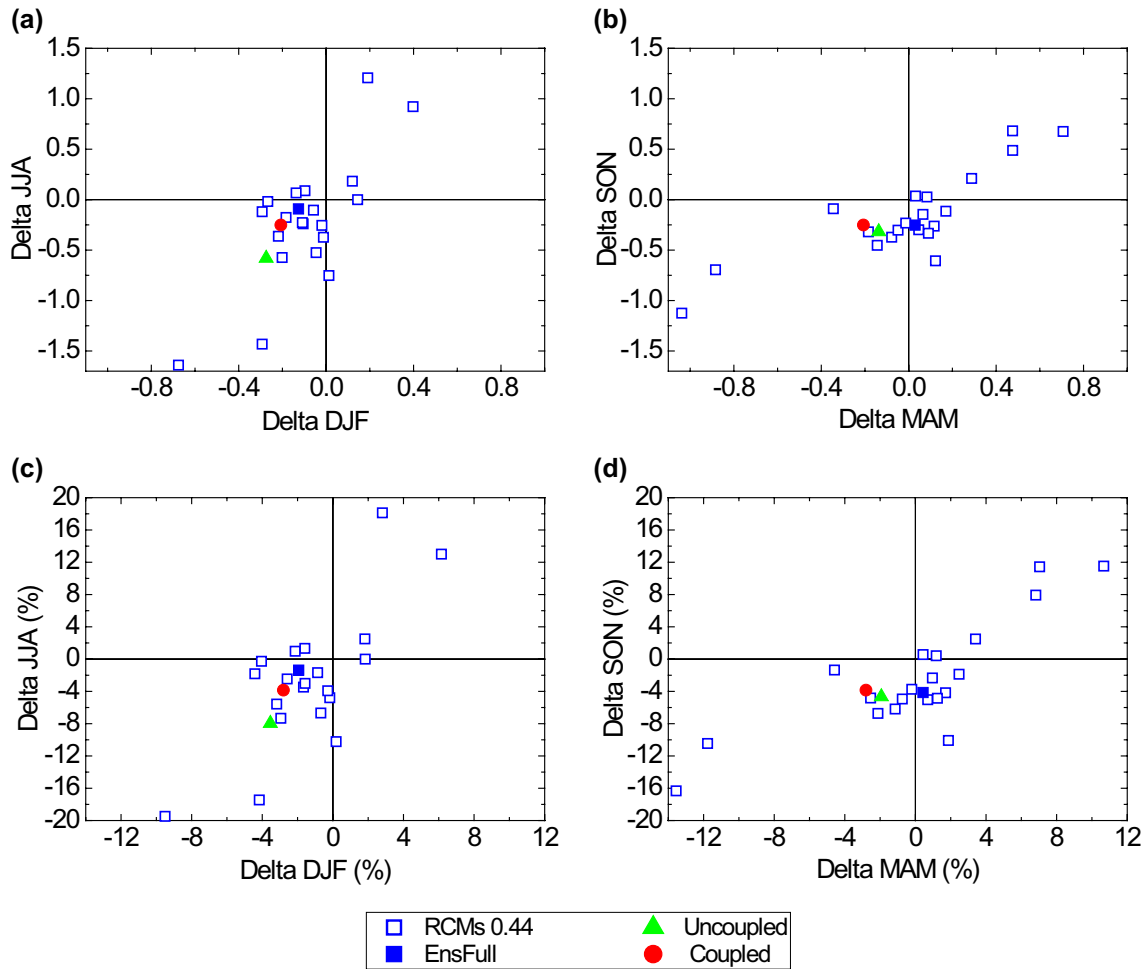


Fig. 7 Surface wind speed delta change values averaged over the domain for the period 2070–2099 with respect to 1976–2005. The delta values are calculated for the seasonal mean values in winter (DJF, X axis) and summer (JJA, Y axis) and in spring (MAM, X axis)

and autumn (SON, Y axis); **a, b** absolute change in m/s and **c, d** relative changes in %. Results given by the ROM simulations (uncoupled and coupled), the CORDEX-Africa full multi-model ensemble mean (EnsFull) and the individual CORDEX-Africa models (RCMs 0.44°)

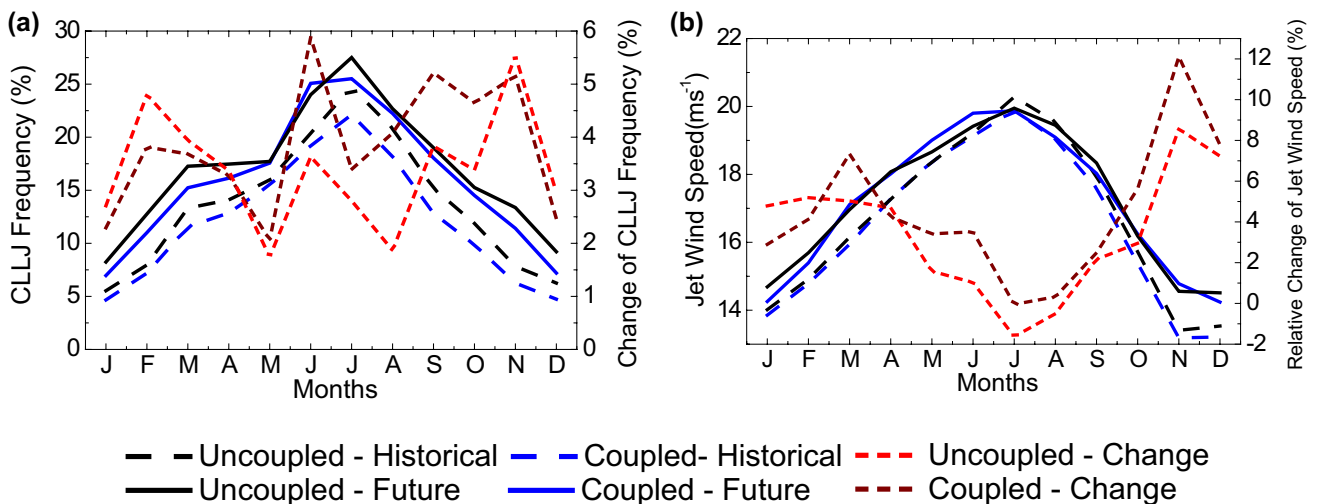


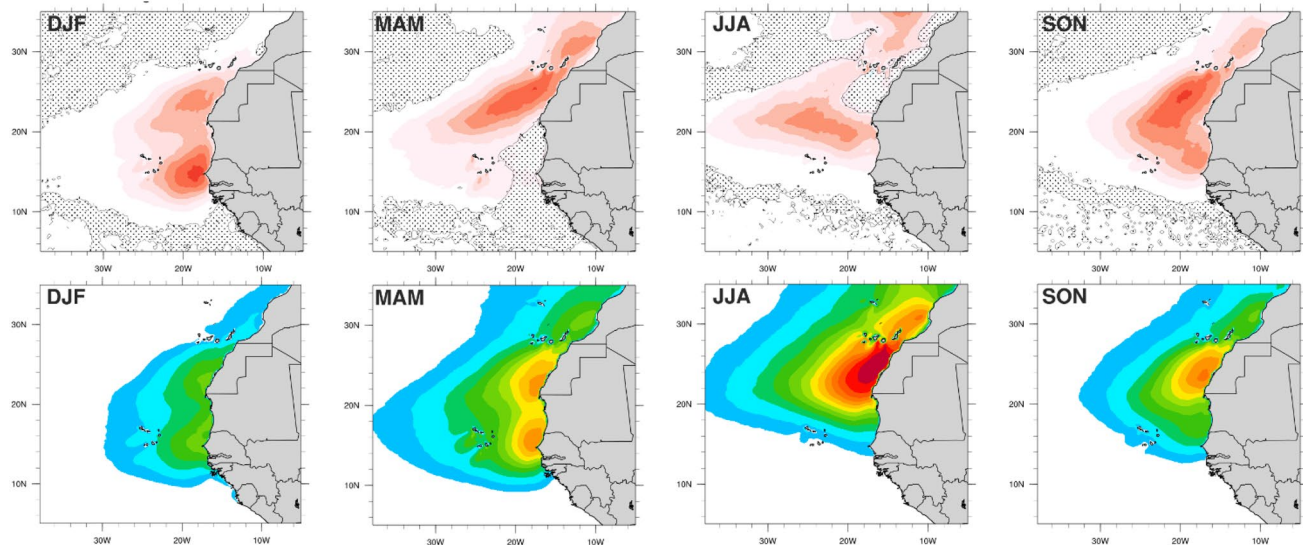
Fig. 8 Annual cycle of the North African coastal low-level jet, **a** the mean jet frequency of occurrence and **b** the mean jet wind speed. Results from the ROM runs (uncoupled and coupled) historical and

future simulations. In the Y-axis the future changes w.r.t. present climate are also shown

In order to offer a spatial view on the NACLLJ pattern projected changes, Fig. 9 depicts the seasonal changes of the jet frequency of occurrence (future minus present) and the future frequencies, from the uncoupled and coupled ROM runs. In the NACLLJ region, both simulations project rises in the frequency of occurrence and, in general, these increases are larger in the coupled run. Only two exceptions appear connected to the southern areas, in the Senegal coast, in winter and autumn. In fact, the seasonal frequencies of the jet intensify for all seasons, which a larger amplification

from spring to autumn. In winter, a significant projected increase of around 10% can be seen in two jet regions: one offshore the Western Sahara and other along the coast of Senegal. These changes are highly significant, since account for projections of almost double of the winter jet persistency and a considerable enlargement of its offshore extension. In spring, the jet frequency changes extend along the full Moroccan and Western Sahara coasts, with maxima around 11 and 15% for the uncoupled and coupled simulations, respectively. In summer, although both runs project higher

ROM-Uncoupled



ROM-Coupled

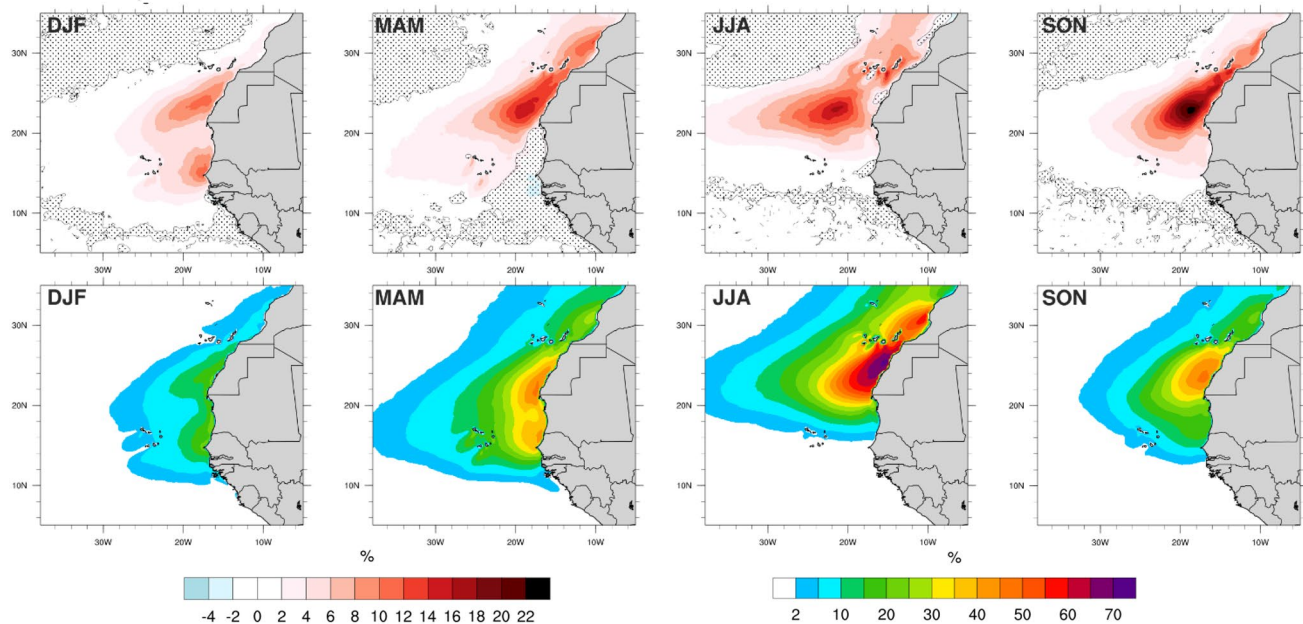


Fig. 9 Maps of seasonal changes of the NACLLJ frequency of occurrence (%) (future–present) (top) and future projections of the NACLLJ frequency of occurrence (%) (bottom), from the ROM

uncoupled and coupled runs. Shaded areas specify changes not statistically significant using a Student’s t-test at the 90% confidence level

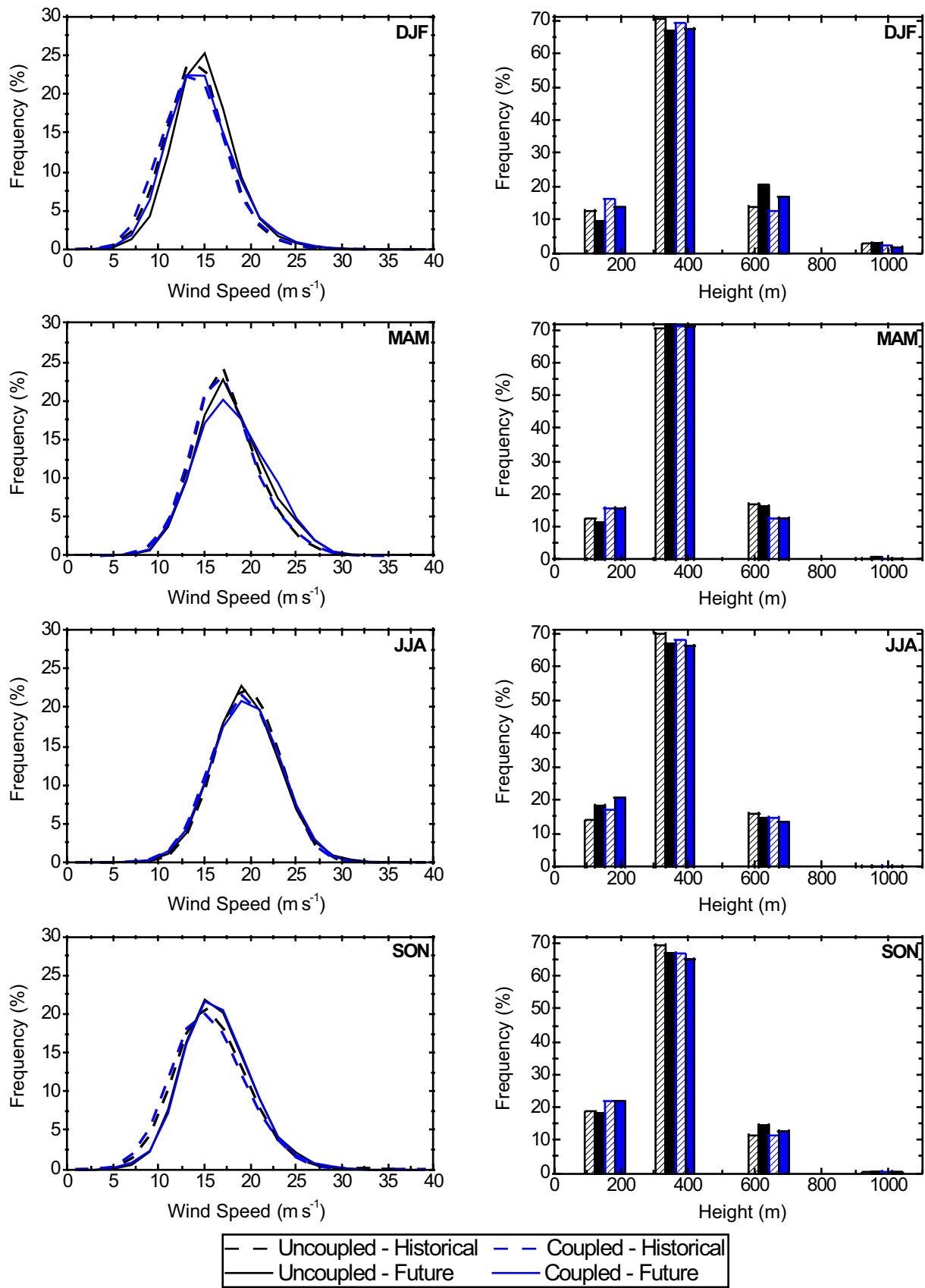


Fig. 10 Seasonal coastal jet wind speed PDFs (left) and jet height histograms (right) from the ROM historical and future simulations (uncoupled and coupled)

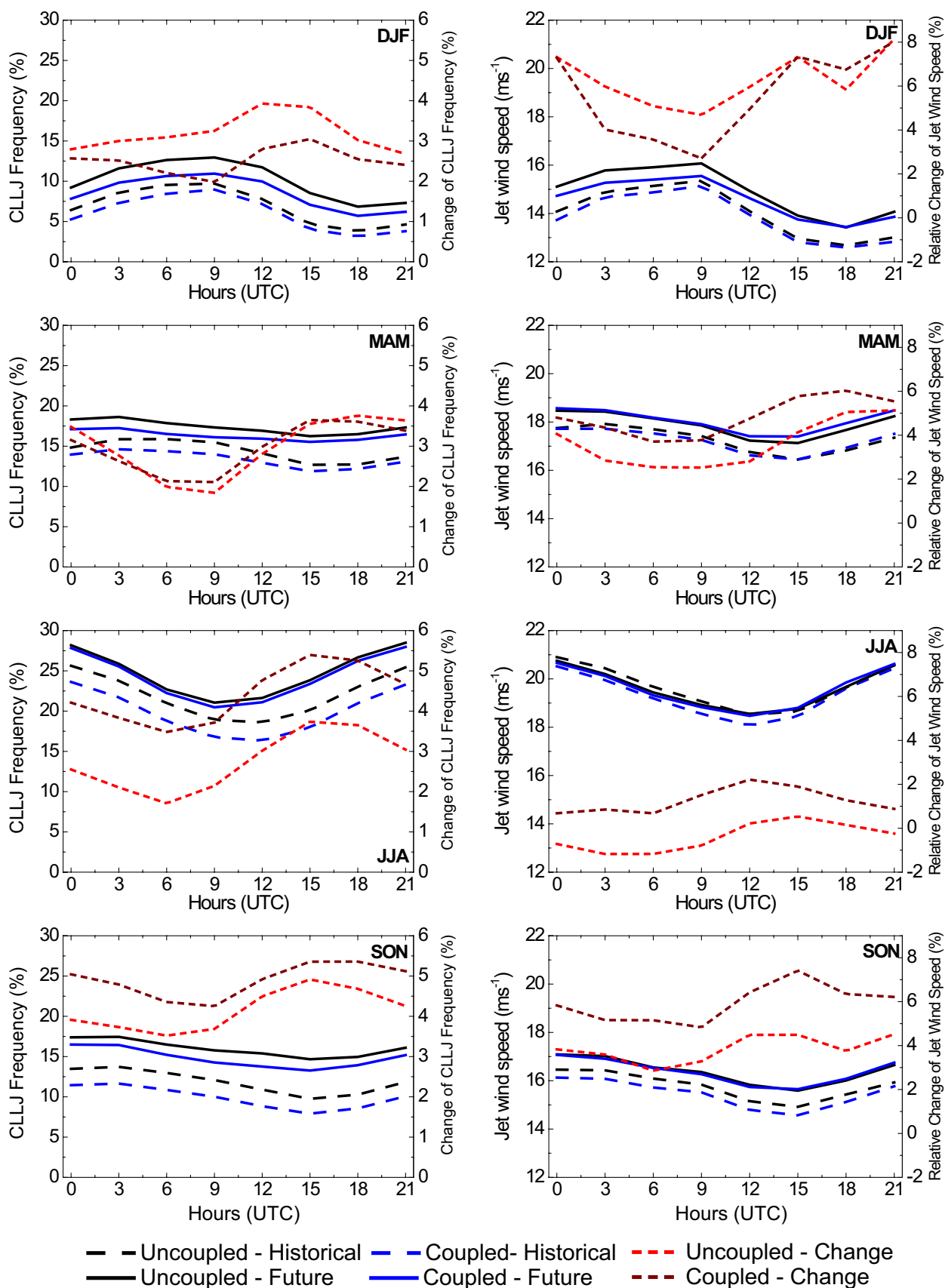


Fig. 11 Diurnal cycles of the coastal jet frequency of occurrence (left) and of the coastal jet wind speed (right) for each season, from the ROM historical and future simulations (uncoupled and coupled). In the Y-axis the future changes w.r.t. present climate are also shown

persistency for the future, the delta changes reveal larger discrepancies and a larger offshore extension. Accordingly, in the uncoupled run the summer frequencies are projected to grow around 10% and in the coupled run around 16%. Note that these maxima are located in offshore areas away from the shore indicating an expansion of the areas under CLLJ. Roughly, this kind of positive deviations is also visible in autumn. For autumn, the uncoupled simulation projects a maximum increase of ~13% and the coupled one ~22%. In the latter case, the rise of the frequency of occurrence corresponds to crudely half of the present-climate frequencies. These areas clearly overlap the zones of lower SST enhancement and thus higher land-sea temperature gradient (not shown).

Figure 9 also displays the regional maps of future seasonal frequencies of occurrence of the NACLLJ, based on the uncoupled and coupled ROM simulations. The NACLLJ projected predominance reveals a strong seasonal cycle with an enhanced persistency all-year-around when compared with present-climate, either historical or hindcast runs (Fig. 4; Soares et al. 2018). The highest coastal jet occurrence still happens in summer, when frequencies of occurrence are projected to reach values over 70%, offshore Western Sahara. Additionally, both in spring and in autumn the coastal jet will be present more than 40% and 50% of the time, respectively. In winter the local maximum frequency is projected to be almost 30%. The horizontal extension of the NACLLJ is likely to include rather vast areas. Generally, the NACLLJ is anticipated to widen up to more than 1500 km offshore, all-year-round. In summer and in autumn the coastal jet covers the offshore areas from north Morocco to central Senegal, and in winter and spring it spreads further south down to the coast of Guinea-Bissau. The frequency maxima roughly follows a similar seasonal cycle. In winter and spring, there is a dipole of maximum values, one in south coastal areas of Western Sahara and a second one in northern Senegal. During summer and autumn there is also a dipole, but a clear maximum offshore Western Sahara is projected to occur. The second local maximum occurs downwind Cape Ghir in southern Morocco. It is noteworthy to emphasize the consistency between the projections of both coupled and uncoupled simulations.

The future changes regarding the jet wind speed (at the jet height) (Fig. 10, left panels) are overall opposite to the surface projections. Figure 10 presents the seasonal frequencies of jet wind speed and jet heights, from the uncoupled and coupled ROM runs, for present and future climates. A shift towards higher jet wind speeds is projected to occur

in winter and in the intermediate seasons, from both ROM simulations. In summer there is a negligible change in the jet wind speed PDFs. Regarding jet heights (Fig. 10, right panels), both ROM projections concur on the increase in altitudes of the NACLLJ occurrence, especially in winter and spring, and, to a lesser extent in autumn and summer. These changes correspond to an increased frequency of jet height events in future climate in a consecutive upper vertical level, when compared to present-climate.

The comparison between the present and future diurnal cycles of NACLLJ frequency of occurrence for each season (Fig. 11, left panels), reveals the overall projected increase of the jet persistency in future climate. This increase in the future does not change to a great extent the diurnal cycle but introduces some small shifts. In fact, in all seasons the increases are larger for the mid- and end afternoon hours than in the night and morning hours. These modifications correspond to slightly different future diurnal cycles in amplitude but not in shape, especially for the coupled ROM run. These changes are especially visible in the flatter diurnal cycles for the future intermediate seasons. The diurnal cycles of the NACLLJ wind speed (Fig. 11, right panels) are projected to undergo similar small increases of wind speeds, throughout the entire day, with the summer season as an exception. In summer, there is hardly any projected change for the future jet wind speeds diurnal cycle. The aforementioned changes are rather consistent between the uncoupled and coupled simulations.

A summary of the NACLLJ projected changes, averaged over the region of interest and in agreement with the RCP8.5 emission scenario is provided in Table 5. As aforementioned, the NACLLJ frequency is projected to intensify consistently in all seasons. In winter, the mean regional values of the coastal jet frequency of occurrence strikingly increase more than 50%, from 6 to 9.3% and from 5 to 7.7%, according to the uncoupled and the coupled ROM runs, respectively. In spring and summer, the estimated relative increases are still important, with values between 13 and 23%. Finally, in autumn the two runs indicate future relative changes in the regional jet occurrence over 35%. The regional average coastal jet wind speeds are projected to change in an opposite manner to the near surface wind speeds (Table 4 and Fig. 5). In fact, the ROM simulations results indicate substantial increases, for future climate, of the regional jet wind speeds for three seasons (DJF, MAM and SON) of around 5%, relatively to present-climate values. For summer, the mean regional jet wind speeds are projected to remain alike. These changes contrast greatly with the above mentioned near surface wind speed decreases, that are projected occur. Pointing out to higher intensities of wind shear in future climate in the NACLLJ region.

Table 5 Mean and inter-annual standard deviations of CLLJ frequency and jet wind speed (seasonal means for the area of interest A marked in Fig. 1b)

			ROM_U historical	ROM_U future	Relative dif- ference (%)	ROM_C historical	ROM_C future	Relative dif- ference (%)
Jet frequency (%)	Mean	DJF	6.02	9.29	54	5.05	7.73	53
		MAM	14.46	17.48	21	13.31	16.31	23
		JJA	21.98	24.74	13	19.83	24.26	22
		SON	11.63	15.87	36	9.65	14.65	52
Jet wind speed (m/s)		DJF	14.11	14.93	6	13.93	14.59	5
		MAM	17.28	17.89	4	17.22	18.04	5
		JJA	19.69	19.61	0	19.35	19.59	1
		SON	15.79	16.39	4	15.46	16.37	6
Jet frequency (%)	Std	DJF	1.52	1.98	30	0.87	1.61	85
		MAM	1.95	2.44	25	1.87	2.28	22
		JJA	1.96	2.89	47	1.80	2.19	22
		SON	1.81	2.05	13	1.69	1.77	5
Jet wind speed (m/s)		DJF	0.67	0.67	0	0.68	0.81	19
		MAM	0.81	0.81	0	0.82	0.88	7
		JJA	0.55	0.67	22	0.53	0.81	53
		SON	0.53	0.58	9	0.75	0.62	-17

Results given by the historical and future ROM simulations (*U* uncoupled and *C* coupled)

Remarkable are also the larger values of inter-annual variability projected for the NACLLJ seasonal frequencies and wind speeds over the region. For all seasons, Table 5 reveals increasing values of standard deviations of the jet frequency, which relatively to present-climate augment between 5% in autumn and 85% in winter, for the ROM coupled simulation. Regarding the seasonal jet wind speeds inter-annual variability, the coupled ROM run projects larger changes compared to the uncoupled simulation. The coupled ROM run projects relative increments in the standard deviations of 19, 7 and 53% in winter, spring and summer, and a decrease for autumn of ~17%. The uncoupled ROM simulation results concerning the changes in the standard deviations for the regional jet wind speeds are diverse, pointing to no changes for future in winter and spring, and increases of ~22 and 9% for summer and autumn, respectively.

5 Conclusions

The EBCS are the most productive fisheries areas in the global Ocean (Wang et al. 2015), hence the evaluation of climate change effects in these areas is of the utmost importance. The main objective of the current study was to investigate the effect of climate change on the spatial and temporal features of the NACLLJ. In order to achieve this goal, two high resolution ROM simulations (uncoupled and coupled to the ocean) and the CORDEX-Africa near surface wind speeds were analyzed for two time periods: 1976–2005 and 2071–2100, the later following the RCP8.5 scenario. The

ROM simulations allowed the detailed depiction of the jet seasonal and diurnal cycles and jet properties (speed, frequency of occurrence, height). The surface wind features were scrutinized in all datasets. An evaluation against observations revealed that the ROM coupled simulation presented the best performance in reproducing the present-day climate, near surface wind speed offshore Northwest Africa, compared to the remaining RCM simulations. The higher SST resolution in the coupled simulations favours colder and much more localised upwelling strips near the coast and consequently stronger jets.

In the future a waning of the near surface wind speed is projected for all seasons in offshore areas in North-western Africa. However, in the coastal regions where the NACLLJ is more persistent some local surface wind speed increase is projected to occur. This is in line with the projected wind speed reductions of Soares et al. (2017a, b). Regarding the coastal jet in a future climate, it is projected to be more frequent, with higher wind speeds and encompassing larger areas. An increase of the jet seasonal frequencies of occurrence is projected for all seasons, which is larger from spring to autumn. The ROM coupled simulation points to an estimated increase of the NACLLJ frequencies of occurrence in some areas, up to 15, 16 and 22%, in spring, summer and autumn, respectively. These increments also extend significantly the spatial coverage of the NACLLJ areas, where higher frequencies of occurrence take place. Moreover, in winter, in some offshore areas, the NACLLJ persistency nearly doubles, relatively to present-climate. Similar results were obtained by Semedo et al. (2016), yet the lower

resolution of the EC-Earth runs project lower frequencies of occurrence and smaller extension. The higher resolution of the WRF simulations in Soares et al. (2017a) provides equally strong augments in CLLJ frequencies offshore of Iberia in summer. The NACLLJ areas, where the largest amplification of the frequency of occurrence is projected, correspond to regions with increased upwelling and thus a higher land–atmosphere temperature gradient (Bakun et al. 2015 and; Wang et al. 2015).

A small shift to higher jet wind speeds is expected to arise in winter and in the intermediate seasons, in both ROM simulations, with future relative increases of ~5% of mean jet wind speed, while a negligible change is anticipated for summer. Both ROM projections concur on the increase in altitudes of the NACLLJ occurrence, especially in winter and spring, and, to a lesser extent in autumn and summer. Higher inter-annual variability is also envisaged for the NACLLJ seasonal frequencies. Additionally, the jet's diurnal cycle shows an increase in jet occurrence across the day, particularly in the mid and late afternoon. A similar result was obtained for Iberia in Soares et al. (2017a) and Cardoso et al. (2016).

The relevant feedbacks between land/ocean and the atmosphere in a CLLJ environment should be targeted in further research, and further coupled simulations with other models should be pursued, in order to assess the uncertainty of the future projections due to different models and emission scenarios. Other features, associated to moisture transport and surface energy fluxes, which are of the outmost relevance to the population living near the coast, will be tackled in a further paper.

Acknowledgements We are grateful to two anonymous reviewers for their very helpful comments. Pedro M.M. Soares, Rita M. Cardoso and A. Semedo wish to acknowledge the SOLAR (PTDC/GEOMET/7078/2014) project. Daniela Lima also thanks the EarthSystems Doctoral Programme at the Faculty of Sciences of the University of Lisbon (Grant PD/BD/106008/2014). These authors also acknowledge the funding by the project FCT UID/GEO/50019/2013—Instituto Dom Luiz. D. Sein's work was supported by the PRIMAVERA project, which has received funding from the European Union's Horizon 2020 research and innovation programme under grant agreement No 641727 and the state assignment of FASO Russia (theme 0149-2019-0015). Finally, all authors acknowledge the German Climate Computing Center (DKRZ) where the ROM simulations were performed; and, are grateful to the World Climate Research Program Working Group on Regional Climate, and the Working Group on Coupled Modelling, former coordinating body of CORDEX and responsible panel for CMIP5. The authors also thank the climate modelling groups (listed in Table 1 of this paper) for producing and making available their CORDEX-Africa model output.

Open Access This article is distributed under the terms of the Creative Commons Attribution 4.0 International License (<http://creativecommons.org/licenses/by/4.0/>), which permits unrestricted use, distribution, and reproduction in any medium, provided you give appropriate credit to the original author(s) and the source, provide a link to the Creative Commons license, and indicate if changes were made.

References

- Atlas R, Hoffman RN, Ardizzone J, Leidner SM, Jusem JC et al (2011) A cross-calibrated, multiplatform ocean surface wind velocity product for meteorological and oceanographic applications. *Bull Am Meteorol Soc* 92:157–174
- Bakun A, Field DB, Redondo-Rodriguez A, Weeks SJ (2010) Greenhouse gas, upwelling-favorable winds, and the future of coastal ocean upwelling ecosystems. *Glob Change Biol* 16:1213–1228. <https://doi.org/10.1111/j.1365-2486.2009.02094.x>
- Bakun A, Black BA, Bograd SJ, García-Reyes M, Miller AJ, Rykaczewski RR, Sydeman WJ (2015) Anticipated effects of climate change on coastal upwelling ecosystems. *Curr Clim Change Rep* 1:85–93. <https://doi.org/10.1007/s40641-015-0008-4>
- Beardsley RC, Dorman CE, Friehe CA, Rosenfield LK, Wynant CD (1987) Local atmospheric forcing during the coastal ocean dynamics experiment 1: a description of the marine boundary layer and atmospheric conditions over a Northern California upwelling region. *J Geophys Res* 92:1467–1488
- Boberg F, Berg P, Thejll P, Gutowski WJ, Christensen JH (2009) Improved confidence in climate change projections of precipitation evaluated using daily statistics from the PRUDENCE ensemble. *Clim Dyn* 32:1097–1106. <https://doi.org/10.1007/s00382-008-0446-y>
- Cabos W, Sein DV, Pinto JG, Fink AH, Koldunov NV, Álvarez F, Izquierdo A, Keenlyside N, Jacob D (2017) The South Atlantic Anticyclone as a key player for the representation of the tropical Atlantic climate in coupled climate models. *Clim Dyn* 48:4051–4069. <https://doi.org/10.1007/s00382-016-3319-9>
- Cardoso RM, Soares PMM, Miranda PMA, Belo-Pereira M (2013) WRF high resolution simulation of Iberian mean and extreme precipitation climate. *Int J Climatol* 33(11):2591–2608. <https://doi.org/10.1002/joc.3616>
- Cardoso RM, Soares PMM, Lima DCA, Semedo A (2016) The impact of climate change on the Iberian low-level wind jet: EURO-CORDEX regional climate simulation. *Tellus A* 68:29005. <https://doi.org/10.3402/tellusa.v68.29005>
- Cardoso RM, Soares PMM, Lima DCA, Miranda PMA (2018) Mean and extreme temperatures in a warming climate: EURO CORDEX and WRF regional climate high-resolution projections for Portugal. *Clim Dyn*. <https://doi.org/10.1007/s00382-018-4124-4>
- Christensen OB, Drews M, Christensen JH, Dethloff K, Ketelsen K, Hebestadt I, Rinke A (2007) The HIRHAM regional climate model version 5 (beta). *Tech Rep* 06(17):1–22
- Christensen J, Kjellstrom E, Giorgi F, Lenderink G, Rummukainen M (2010) Weight assignment in regional climate models. *Clim Res* 44:179–194
- Dee DP et al (2011) The ERA-Interim reanalysis: configuration and performance of the data assimilation system. *Q J R Meteorol Soc* 137:553–597
- Ferro CAT, Hannachi A, Stephenson DB (2005) Simple nonparametric techniques for exploring changing probability distributions of weather. *J Clim* 18:4344–4354. <https://doi.org/10.1175/JCLI3518.1>
- Giorgetta MA et al (2013) Climate and carbon cycle changes from 1850 to 2100 in MPI-ESM simulations for the Coupled Model Intercomparison Project phase 5. *J Adv Model Earth Syst* 5:572–597. <https://doi.org/10.1002/jame.20038>
- Giorgi F, Jones C, Asrar GR (2009) Addressing climate information needs at the regional level: the CORDEX framework. *Bull World Meteorol Organ* 58:175–183
- Hewitson B, Lennard C, Nikulin G, Jones C (2012) CORDEX-Africa: a unique opportunity for science and capacity building CLIVAR. *Exchanges* 60:6–7

- Jacob D et al (2001) A comprehensive model inter-comparison study investigating the water budget during the BALTEX-PIDCAP period. *Meteorol Atmos Phys* 77:19–43. <https://doi.org/10.1007/s007030170015>
- Li H, Kanamitsu M, Hong S-Y (2012) California reanalysis downscaling at 10 km using an ocean-atmosphere coupled regional model system. *J Geophys Res* 117:D12118. <https://doi.org/10.1029/2011JD017372>
- Lima D, Soares PMM, Semedo A, Cardoso RM (2017) A global view of coastal low-level wind jets using an ensemble of reanalysis. *J Clim*. <https://doi.org/10.1175/JCLI-D-17-0395.1>
- Nogueira M, Soares PMM, Tomé R, Cardoso RM (2018) High-resolution multi-model projections of onshore wind resources over Portugal under a changing climate. *Theoret Appl Climatol*. <https://doi.org/10.1007/s00704-018-2495-4>
- Paeth H, Paxian A, Sein D, Jacob D, Panitz HJ, Warscher M, Fink A, Kunstmann H, Breil M, Engel T, Krause A, Tödter J, Ahrens B (2017) Decadal and multi-year predictability of the West African monsoon and the role of dynamical downscaling. *Meteorol Z* 26(4):363–377
- Patricola CM, Chang P (2017) Structure and dynamics of the Benguela low-level coastal jet. *Clim Dyn* 49(7–8):2765–2788. <https://doi.org/10.1007/s00382-016-3479-7>
- Pauly D, Christensen V (1995) Primary production required to sustain global fisheries. *Nature* 374:255–257
- Paxian A, Sein D, Panitz HJ, Warscher M, Breil M, Engel T, Tödter J, Krause A, Narvaez C, Fink W, Ahrens A, Kunstmann B, Jacob HD, Paeth H (2016) Bias reduction in decadal predictions of West African monsoon rainfall using regional climate models. *J Geophys Res Atmos* 121:1715–1735
- Ranjha R, Svensson G, Tjernström M, Semedo A (2013) Global distribution and seasonal variability of coastal low-level jets derived from ERA-Interim reanalysis. *Tellus A* 65:20412
- Ranjha R, Tjernström M, Semedo A, Svensson G, Cardoso RM (2015) Structure and variability of the Oman coastal low-level jet. *Tellus Ser A Dyn Meteorol Oceanogr* 67(1):1–20. <https://doi.org/10.3402/tellusa.v67.25285>
- Reynolds RW, Smith TM, Liu C, Chelton DB, Casey KS, Schlax MG (2007) Daily high-resolution-blended analyses for sea surface temperature. *J Clim* 20:5473–5496. <https://doi.org/10.1175/2007jcli1824.1>
- Riahi K, Rao S, Krey V, Cho C, Chirkov V, Fischer G, Kindermann G, Nakicenovic N, Rafaj P (2011) RCP 8.5—a scenario of comparatively high greenhouse gas emissions. *Clim Change* 109:33–57. <https://doi.org/10.1007/s10584-011-0149-y>
- Rijo N, Lima DCA, Semedo A, Miranda PMA, Cardoso RM, Soares PMM (2017) Spatial and temporal variability of the Iberian Peninsula coastal low-level jet. *Int J Climatol*. <https://doi.org/10.1002/joc.5303>
- Rockel B, Will A, Hense A (2008) The regional climate modelling with COSMO-CLM (CCLM). *Meteorologische Z* 17(4):347–348 (**Special issue**)
- Samuelsson P et al (2011) The Rossby centre regional climate model RCA3: model description and performance. *Tellus Ser A Dyn Meteorol Oceanogr* 63:4–23. <https://doi.org/10.1111/j.1600-0870.2010.00478.x>
- Savijärvi H, Niemelä S, Tisler P (2005) Coastal winds and low level jets: simulations for sea gulfs. *Q J R Meteorol Soc* 131:625–637
- Schulzweida U, Kornbluh L, Quast R (2006) CDO user's guide. Climate data operators, Version 1(6)
- Sein D, Koldunov N, Pinto J, Cabos W (2014) Sensitivity of simulated regional Arctic climate to the choice of coupled model domain. *Tellus A* 66:23966. <https://doi.org/10.3402/tellusa.v66.23966>
- Sein DV, Mikolajewicz U, Gröger M, Fast I, Cabos W, Pinto JG, Hagemann S, Semmler T, Izquierdo A, Jacob D (2015) Regionally coupled atmosphere-ocean-sea ice-marine biogeochemistry model ROM: 1. Description and validation. *J Adv Model Earth Syst* 7:268–304. <https://doi.org/10.1002/2014MS000357>
- Semedo A, Soares PMM, Lima DCA, Cardoso RM, Bernardino M, Miranda PMA (2016) The impact of climate change on the global coastal low-level wind jets: EC-EARTH simulations. *Global Planet Change* 137:88–106
- Snyder MA, Sloan LC, Diffenbaugh NS, Bell JL (2003) Future climate change and upwelling in the California current. *Geophys Res Lett* 30:1823. <https://doi.org/10.1029/2003GL017647>
- Soares PMM, Cardoso RM (2017d) A simple method to assess the added value using high-resolution climate distributions application to the EURO-CORDEX daily precipitation. *Int J Climatol*. <https://doi.org/10.1002/joc.5261>
- Soares PMM, Cardoso RM, Miranda PMA, De Medeiros J, Belopereira M et al (2012) WRF high resolution dynamical downscaling of ERA-Interim for Portugal. *Clim Dyn* 39:24972522. <https://doi.org/10.1007/s00382-012-1315-2>
- Soares PMM, Cardoso RM, Semedo A, Chinita MJ, Ranjha R (2014) Climatology of the Iberia coastal low-level wind jet: weather research forecasting model high-resolution results. *Tellus A* 66:22377
- Soares PMM, Cardoso RM, Ferreira JJ, Miranda PMA (2015) Climate change and the Portuguese precipitation: ENSEMBLES regional climate model results. *Clim Dyn* 45(7):1771–1787. <https://doi.org/10.1007/s00382-014-2432-x>
- Soares PMM, Lima DCA, Cardoso RM, Semedo A (2017a) High resolution projections for the western Iberian coastal low level jet in a changing climate. *Clim Dyn*. <https://doi.org/10.1007/s00382-016-3397-8>
- Soares PMM, Lima DCA, Cardoso RM, Nascimento M, Semedo A (2017b) Western Iberian offshore wind resources: more or less in a global warming climate? *Appl Energy* 203:72–90. <https://doi.org/10.1016/j.apenergy.2017.06.004>
- Soares PMM, Cardoso RM, Lima DCA, Miranda PMA (2017c) Future precipitation in Portugal: high-resolution projections using WRF model and EURO-CORDEX multi-model ensembles. *Clim Dyn* 49:2503–2530. <https://doi.org/10.1007/s00382-016-3455-2>
- Soares PMM, Lima DCA, Semedo A, Cardoso RM, Cabos W, Stein D (2018) The North African coastal low level jet—a high resolution view. *Clim Dyn*. <https://doi.org/10.1007/s00382-018-4441-7>
- Suklitsch M, Gobiet A, Leuprecht A, Frei C (2008) High resolution sensitivity studies with the regional climate model cclm in the alpine region. *Meteorol Z* 17:467–476
- Tang WQ, Liu WT, Stiles BW (2004) Evaluations of high resolution ocean surface vector winds measured by QuikSCAT scatterometer in coastal regions. *IEEE Trans Geosci Rem Sens* 42:17621769
- van Meijgaard E, Van Uft LH, Van De Berg WJ, Bosveld FC, Van Den Hurk BJM, Lenderink G, Siebesma AP (2008) The KNMI regional atmospheric climate model RACMO version 2.1
- Wang D, Gouhier TC, Menge BA, Ganguly AR (2015) Intensification and spatial homogenization of coastal upwelling under climate change. *Nature* 518:390–394
- Wilks DS (2006) *Statistical methods in the atmospheric sciences*. Academic Press, New York, p 676
- Willmott CJ, Robeson SM, Matsuura K (2012) A refined index of model performance. *Int J Climatol* 32:2088–2094. <https://doi.org/10.1002/joc.2419>
- Winant CD, Dorman CE, Friehe CA, Beardsley RC (1988) The marine layer off northern California: an example of supercritical channel flow. *J Atmos Sci* 45:3588–3605

Publisher's Note Springer Nature remains neutral with regard to jurisdictional claims in published maps and institutional affiliations.